

Finite-size scaling of geometric renormalization flows in complex networks

Dan Chen^a, Housheng Su^{a,*}, Xiaofan Wang^b, Gui-Jun Pan^c, Guanrong Chen^d

^a*School of Artificial Intelligence and Automation, Image Processing and Intelligent Control Key Laboratory of Education Ministry of China, Huazhong University of Science and Technology, Wuhan, 430074, China*

^b*Department of Automation, Shanghai University, Shanghai 200072, China*

^c*Faculty of Physics and Electronic Science, Hubei University, Wuhan 430062, China*

^d*Department of Electrical Engineering, City University of Hong Kong, Hong Kong, China*

Abstract

Recently, the concept of geometric renormalization group provides a good approach for studying the structural symmetry and functional invariance of complex networks. Along this line, we systematically investigate the finite-size scaling of structural and dynamical observables in geometric renormalization flows of synthetic and real evolutionary networks. Our results show that these observables can be well characterized by a certain scaling function. Specifically, we show that the critical exponent implied by the scaling function is independent of these observables but only depends on the small-world properties of the network, namely, all networks located in the small-world phase have a uniform scaling exponent, while those located in the non-small-world phase and in their critical regions have another uniform scaling. More importantly, we perform extensive experiments on real evolutionary networks with small-world characteristics, and our results show that these observables also have uniform scaling in their geometric renormalization flows. Therefore, in a sense this exponent can be used as an effective measure for classifying universal small-world and non-small-world network models.

Introduction

Complex networks have attracted considerable attention from various disciplines such as mathematics, physics, biology, engineering, computer science, and so on [1]. Its emergence was due to the discovery that associated with a real system there exists a corresponding network which can well define the interactions among the system components [2]. Because of this, one can better understand the structural and functional properties of the real system. In particular, by studying the topology of the network associated with a real system, some small-world properties [3] and scale-free properties [4] were identified. Consequently, their functional performances could be further studied, including synchronization [5, 6], observability and controllability [7, 8], reaction-diffusion [9], navigation [10], transportation [11, 12], and many other dynamic behaviors.

*Corresponding author: shs@hust.edu.cn

However, exploring the network structural and functional properties also faces many challenges. For example, the evolutions of real-world networks usually lead to more complicated interactions and increasing numbers of nodes and edges, causing more difficulties to the investigations. In the past two decades, the renormalization technique [13, 14] was found to be very effective for tackling the troublesome problem. This framework significantly reduces the size and the complexity of a large-scale network by retaining the “slow” degrees of freedom in the network, while integrating the rest together. In so doing, smaller networks can be used to approximate the initially large ones. By performing a coarse-graining procedure for a spatially embedded scale-free network, it was shown [15] that a smaller network can maintain important structural characteristics of the original one. Based on random walks, a coarse-graining method was proposed [16] to reduce the size of a network, but retain most spectral properties of the original network through an iteration process. Furthermore, using the shortest path-length measure of a network, a box-covering technique was presented [17–19] for reducing the size of the network. It was shown that the iteration process can keep an approximately identical degree distribution of the network, which was verified by some real-world networks. Such a property is known as the network self-similarity [17]. In the following years, the box-covering technique had significant influences on the research of fractality and self-similarity [20–22], as well as flows and fixed points [23–25], of various complex networks.

It was observed that, for networks with small-world or even ultrasmall-world properties, the transformation method based on shortest path-length cannot be effectively applied to study their structural symmetry and functional invariance. Therefore, a geometric renormalization (GR) framework was proposed [26], embedded in a hidden metric space [27–32], which provides deep insights for studying the structural symmetry of complex networks. This framework is proved capable of preserving both structural and dynamical characteristics of scale-free networks, such as degree distribution, clustering spectrum, dynamics, and navigability, to a certain extent of accuracy within an appropriate number of iterations. Due to the finite-size effect on such networks, however, excessive GR iterations will eventually result in a large deviation of the network features from the original ones.

To further explore the variation of the characteristics of a network in the GR iteration process, this paper reports a comprehensive study of the finite-size scaling (FSS) behavior of the structural and dynamical observables in renormalization flows of synthetic and real evolutionary networks. Specifically, we consider networks in small-world phase, non-small-world phase, and their critical regions, respectively, and perform FSS analyses of their structural and dynamic observables. Our results show that these observables can be characterized by a certain scaling function, and the exponent implied by the scaling function is independent of these observables but only depends on the characteristics of the small-world structure of the network. We have verified the effectiveness of this conclusion via some real evolutionary networks, which further provides evidence for the predictive power of synthetic models to real systems.

Geometric renormalization group and observables of the network

We carry out a comprehensive study of the finite-size scaling (FSS) behavior of the structural and dynamical observables in renormalization flows of the typical \mathbb{S}^1 geometric network

model [27]. This model is generated by two mechanisms of popularity and similarity dimensions [30], which can clearly explain some universal properties of real networks, regarding their structural complexity, evolutionary mechanism, and dynamic behavior. First, an \mathbb{S}^1 network is generated with N_0 nodes and E_0 edges, denoted as G_0 . Then, starting from G_0 , non-overlapping blocks of continuous nodes of size s are defined in the \mathbb{S}^1 circle [26]. Here, $s = 2$ is chosen, and one-step GR iteration is performed to obtain G_1 . Consecutively, a layer- l renormalized network G_l is obtained after l steps of GR iterations. The number of nodes in layer l is denoted by N_l , and the relative network size of layer l is $n_l = N_l/N_0$. Recall that the GR transformation has a good characteristic that it can well predict the average degree of a large-scale network in the process of GR iterations. Taking the \mathbb{S}^1 model for example, it was shown [26] that the average degree can satisfactorily approximate the exponential relation through the GR flows, with $\langle k \rangle_l = s^\alpha \langle k \rangle_{l-1}$, where $\langle k \rangle_l$ is the average degree of the renormalized network G_l , and the exponent α depends on the structural parameters ν and σ of the \mathbb{S}^1 model (see Supplementary Information for notations and descriptions). With respect to different phases of structural and dynamical behaviors, the \mathbb{S}^1 model can be roughly divided into three regions [26] (see section II in the Supplementary Information), denoted as **I**, **II**, and **III**, respectively. In regions **I** and **III**, which correspond to the small-world phase, $\langle k \rangle_l$ approximates an exponential growth. In region **II**, which corresponds to the non-small-world phase, $\langle k \rangle_l$ approximates an exponential decay, where the structure of the renormalized network is similar to a ring as a fixed point. At the edge of the transition between regions **I** and **II**, $\langle k \rangle_l$ presents a tendency of slow increase with the increase of l , which gradually becomes saturated (see Supplementary Information Fig. S1 for details).

In the following, a GR flow is tracked by eight observables. One is the normalized maximum degree of the renormalized network,

$$k_{l,\max} = \frac{K_l}{N_l - 1}, \quad (1)$$

where K_l is the maximum degree of the renormalized network G_l , and $N_l - 1$ is the maximum value that K_l may take. Another observable is the normalized average degree,

$$\langle k \rangle_{l,n} = \frac{\langle k \rangle_l}{N_l - 1}, \quad (2)$$

where $N_l - 1$ is the maximum value that $\langle k \rangle_l$ may take. The average clustering coefficient $\langle c \rangle_l$ and the average shortest path-length $\langle \ell \rangle_l$ for the renormalized network G_l will also be considered below.

Regarding the above characteristics of networks, the FSS behavior is investigated through a box-covering procedure [23, 24]. These observables are commonly used to characterize the basic topological properties of the network, referred to as topological observables of the network, as illustrated in Fig. 1.

Now, consider several other observables that represent global properties of networks. One is the normalized maximum eigenvalue of the Laplace matrix,

$$\lambda_{l,n}(L) = \frac{\Lambda_{l,n}(L)}{N_l}, \quad (3)$$

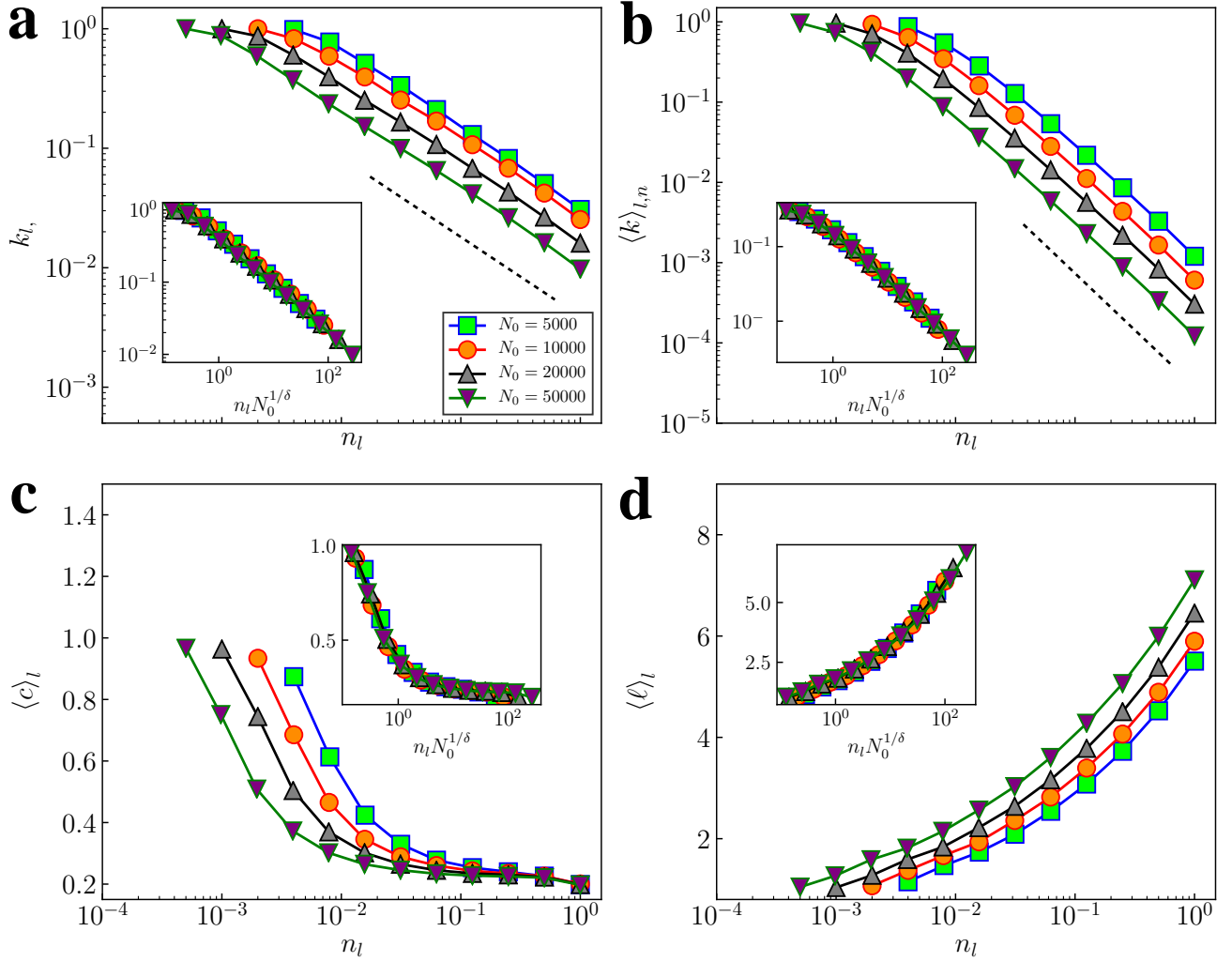


Figure 1: FSS analysis of \mathbb{S}^1 -network topological observables along the GR flow. The main figures show each observable as a function of the variable n_l in the process of GR transformation, and the inset shows their scaling functions related to the variable $n_l N_0^{1/\delta}$. Key parameters of the \mathbb{S}^1 network are $\nu = 2.5$ and $\sigma = 1.5$, respectively; the scaling exponent corresponding to four observables is $\delta = 2 \pm 0.1$. For observables $k_{l,max}$ and $\langle k \rangle_{l,n}$, the black dashed-lines predict their power-law behavior. The average hidden degree $\langle \kappa \rangle_0 \approx 6$ and the expected average degree $\langle k \rangle_0 \approx 6$ for all initial networks. All the results are averaged over 10 independent realizations.

where $\Lambda_{l,n}(L)$ is the maximum eigenvalue of the Laplace matrix L of the renormalized network G_l , and N_l is the maximum value that $\Lambda_{l,n}(L)$ may take. For a connected network with at least one edge, it always satisfies $\Lambda_{l,n}(L) \geq K_l + 1$, where the equality holds if and only if $K_l = N_l - 1$ [33]. The first normalized nonzero eigenvalue of the Laplace matrix is

$$\lambda_{l,2}(L) = \frac{\Lambda_{l,2}(L)}{N_l}, \quad (4)$$

where $\Lambda_{l,2}(L)$ is the first nonzero eigenvalue of the Laplace matrix L of the renormalized network

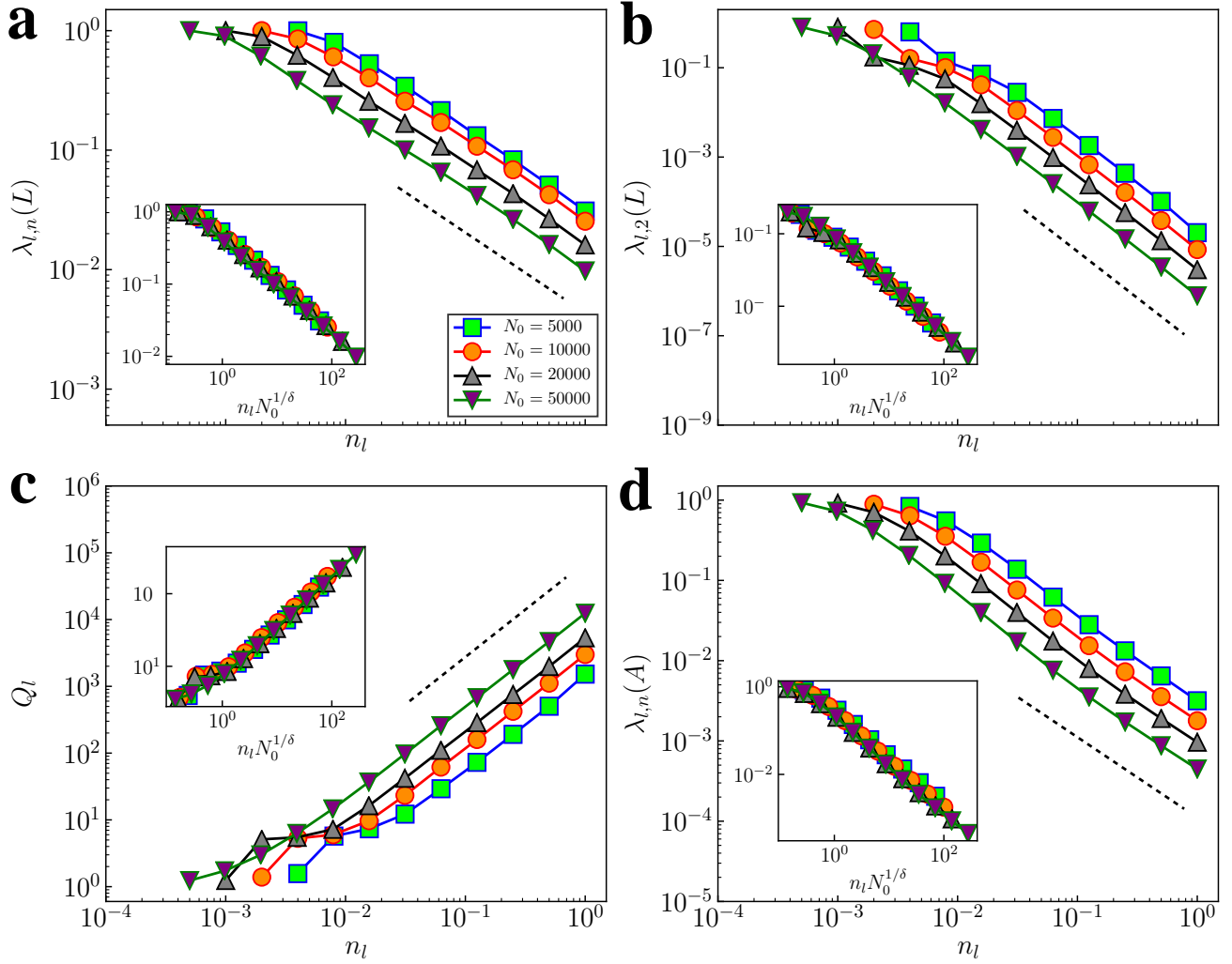


Figure 2: FSS analysis of \mathbb{S}^1 -network dynamic observables along the GR flow. The main figures show each observable as a function of the variable n_l in the process of GR transformation, and the inset shows their scaling functions related to the variable $n_l N_0^{1/\delta}$. Key parameters of the \mathbb{S}^1 network are $\nu = 2.5$ and $\sigma = 1.5$, respectively; the scaling exponent corresponding to four observables is $\delta = 2 \pm 0.1$. For all observables, the black dashed-lines predicted their power-law behavior. The average hidden degree $\langle \kappa \rangle_0 \approx 6$ and the expected average degree $\langle k \rangle_0 \approx 6$ for all initial networks. All the results are averaged over 10 independent realizations.

G_l , and N_l is the maximum value that $\Lambda_{l,2}(L)$ may take. To some extent, the functional properties of a network can be optimized by increasing the value of $\Lambda_{l,2}(L)$. For instance, maximizing $\Lambda_{l,2}(L)$ can maximize the rate of convergence to the network homogeneous state for undirected networks [34].

Also, the \mathbb{S}^1 model parameters can be divided into three regions according to the diffusion time $1/\Lambda_{l,2}(L)$ as discussed before [26]. In the following, consider the ratio of the maximum

eigenvalue of the Laplace matrix to the first nonzero eigenvalue [35–40],

$$Q_l = \frac{\lambda_{l,n}(L)}{\lambda_{l,2}(L)}, \quad (5)$$

which is related to the synchronizability [35, 41] and stability [26] of the network synchronization process.

Lastly, the spectral properties of the network adjacency matrix determine the behavior of many dynamic processes, among which the largest eigenvalue of the adjacency matrix is an important one, and its normalized result is given by

$$\lambda_{l,n}(A) = \frac{\Lambda_{l,n}(A)}{N_l - 1}, \quad (6)$$

where $\Lambda_{l,n}(A)$ is the largest eigenvalue of the adjacency matrix A of G_l , and $N_l - 1$ is the maximum value that $\Lambda_{l,n}(A)$ may take. Recently, the relationship between the maximum eigenvalue $\Lambda_{l,n}(A)$ and two network subgraphs is revealed for a large number of synthetic and real networks [42]. It also shows [43] the impact of $\Lambda_{l,n}(A)$ on two highly correlated dynamical models, one is epidemic spreading with threshold $\lambda_c = 1/\Lambda_{l,n}(A)$ and the other is synchronization of Kuramoto oscillators with threshold $\zeta_c = \zeta_0/\Lambda_{l,n}(A)$. In this context, the variables in Eqs. (3)–(6) have a critical effect on the dynamical behavior of the network. For this reason, they are called dynamic observables of networks. Their FSS is shown in Fig. 2.

Next, along the directions of the GR flows, FSS analysis is performed on eight network observables in regions **I** (small-world phase) and **II** (non-small-world phase), respectively. Specifically, the dependence of these observables on n_l is investigated for each layer of the renormalized network. The results indicate that these observables can be represented by a scaling function with $n_l N_0^{1/\delta}$ as the variable. More precisely, any observable \mathcal{X} approximately satisfies

$$\mathcal{X} = f\left(n_l N_0^{1/\delta}\right), \quad (7)$$

where $f(\cdot)$ is a function depending on the initial network size and specific transformation used.

Results

FSS of GR flows in synthetic networks. Figure 1 shows the dependence of $k_{l,\max}$, $\langle k \rangle_{l,n}$, $\langle c \rangle_l$ and $\langle \ell \rangle_l$ on n_l for the \mathbb{S}^1 synthetic network. The inset shows each observable as a function of $n_l N_0^{1/\delta}$. The results show that the observable curves of networks with different sizes largely overlap. Specifically, in the small-world phase with $(\nu, \sigma) = (2.5, 1.5)$, the scaling exponent $\delta \approx 2$ (see Fig. 1), while in the non-small-world phase with $(\nu, \sigma) = (3.5, 2.5)$, the scaling exponent $\delta \approx 1$ (see Supplementary Information Fig. S4). This appears to be true also when the values of (ν, σ) are taken elsewhere in each phase (see Supplementary Information Table S1 for details). Interestingly, for $k_{l,\max}$ and $\langle k \rangle_{l,n}$, the results shown in Fig. 1 demonstrate that they are both approximately obey a power-law relationship with n_l , where the black dashed-lines predict their power-law behavior.

In the following, the power-law behaviors of these two observables are further discussed. Simulation results show that the maximum degree K_l of the renormalized network G_l and the maximum degree K_{l-1} of G_{l-1} are related as

$$K_l = s^\varepsilon K_{l-1} = \cdots = s^{l\varepsilon} K_0. \quad (8)$$

Since $n_l = N_l/N_0 = s^{-l}$, it follows that

$$\begin{aligned} k_{l,\max} &= \frac{K_l}{N_l - 1} \approx \frac{s^{l\varepsilon} K_0}{N_l} = \frac{n_l^{-\varepsilon} K_0}{n_l N_0} \\ &= \frac{n_l^{-(\varepsilon+1)} K_0}{N_0} \\ &\approx k_{0,\max} n_l^{-(\varepsilon+1)}. \end{aligned} \quad (9)$$

The above equation indicates that $k_{l,\max}$ approximately follows a power-law relation, $k_{l,\max} \sim n_l^{-\beta}$, where $\beta = \varepsilon + 1$. For the observed average degree $\langle k \rangle_l$ of the renormalized network G_l , when $\nu - 1 < 2\sigma$, it was shown [26] that the average degree approximately satisfies an exponential relation along the GR flow, $\langle k \rangle_l = s^\alpha \langle k \rangle_{l-1}$, which yields

$$\langle k \rangle_l = s^\alpha \langle k \rangle_{l-1} = \cdots = s^{l\alpha} \langle k \rangle_0, \quad (10)$$

consequently,

$$\begin{aligned} \langle k \rangle_{l,n} &= \frac{\langle k \rangle_l}{N_l - 1} \approx \frac{s^{l\alpha} \langle k \rangle_0}{N_l} = \frac{n_l^{-\alpha} \langle k \rangle_0}{n_l N_0} \\ &= \frac{n_l^{-(\alpha+1)} \langle k \rangle_0}{N_0} \\ &\approx \langle k \rangle_{0,n} n_l^{-(\alpha+1)}. \end{aligned} \quad (11)$$

The above equation shows that, when $\nu - 1 < 2\sigma$, $\langle k \rangle_l$ approximately obeys a power-law relation, $\langle k \rangle_{l,n} \sim n_l^{-\eta}$, with $\eta = \alpha + 1$. For $\nu - 1 > 2\sigma$, through simulations it is found that the average degree $\langle k \rangle_l$ still approximately satisfies $\langle k \rangle_l = s^\alpha \langle k \rangle_{l-1}$, leading to $\langle k \rangle_{l,n} \sim n_l^{-\eta}$, with $\eta = \alpha + 1$. The values of β and η are given in the Supplementary Information Table S2.

Finally, consider the dependence of several dynamic observables on n_l (see Eqs. (3)–(6)), which depend on the spectral properties of the Laplace matrix and the adjacency matrix of the network, as shown in Fig. 2. To a certain extent, these observables are able to reflect some dynamical properties of a network, such as synchronization stability, diffusion time, and synchronization threshold of Kuramoto oscillator parameters. The inset of Fig. 2 shows the dependence of the observables on $n_l N_0^{1/\delta}$ for different sizes of networks, which is similar to the phenomenon presented in Fig. 1. More importantly, the exponent δ is also consistent with that in Fig. 1, namely, in the small-world phase, $\delta \approx 2$, and in the non-small-world phase, $\delta \approx 1$ (see Supplementary Information Fig. S5). The black dashed-line predicts the power-law behavior of each observable along the GR flow. The corresponding power-law exponent values are

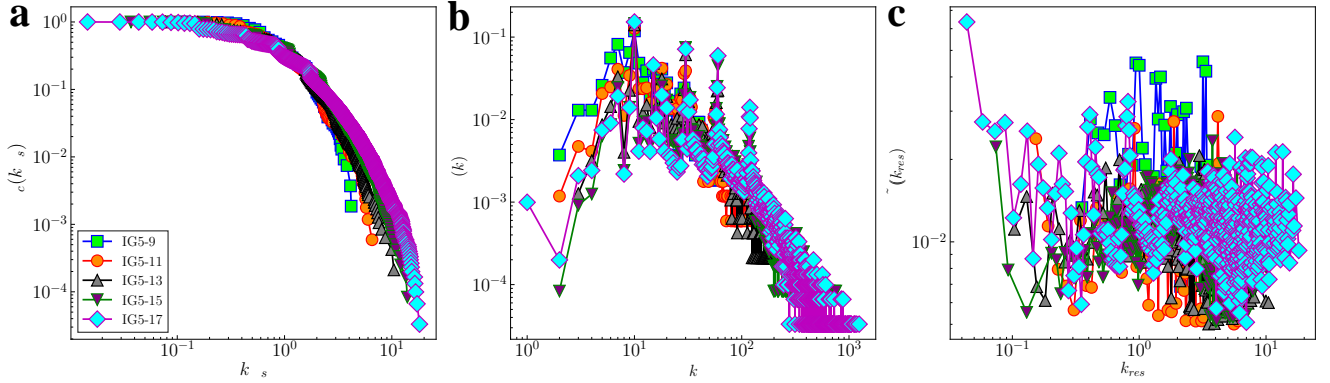


Figure 3: Self-similarity of IG5 evolutionary networks. a The complementary cumulative distribution function (CCDF) P_c of node rescaled degrees $k_{res} = k/\langle k \rangle$. b The probability distribution function (PDF) $P(k)$ of the degree of nodes. c The degree-dependent clustering coefficient $\tilde{C}(k_{res})$ of node rescaled degrees k_{res} . Topological characteristics of this series of evolutionary networks are given in Supplementary Information Table S3.

listed in the Supplementary Information Table S2. It is worth noting that these observables approximately obey power-law curves along the GR flows, providing important guidance for predicting the structural and dynamical properties of large-scale networks. For instance, one can use the eigenvalue ratio Q_l of a renormalized smaller-size network to estimate the synchronizability of the initial large-scale network. To some extent, it can also be used to eliminate various consequences caused by the high complexity of large-scale networks. Furthermore, the results also show that for higher-dimensional embedded networks, by embedding a network into a D -dimensional ($D \geq 2$) space, the value of the exponent δ is consistent with that of the \mathbb{S}^1 model (see Supplementary Information Figs. S8-S11).

FSS of GR flows in real evolutionary networks. As a common practice, it is necessary to verify the universality of the above conclusions with real networks, mostly small-world networks. Obviously, this brings up the problem that a single network has only one initial size N_0 . To address this issue, some evolutionary network systems are employed, each of which eventually leads to a series of networks of different sizes over time, and these networks of the same type with different sizes are all approximately in the same phase on the (ν, σ) plane. Ten types of real evolutionary networks [44–48] (including 39 networks) are investigated and the parameter σ value of each network is inferred according to an existing method [49]. The results show that these networks belong to small-world networks, that is, in phase **I** or **III**.

These networks are then embedded into different \mathbb{S}^1 networks and then the geometric renormalization transformation is performed. It is found that the eight observables curves of the same type but different sizes of the evolutionary networks overlap roughly, and the exponent δ is consistent with that of the synthetic network (small-world phase), i.e., $\delta \approx 2$. Take the IG5 evolutionary network [44] as an example. It has five different system sizes at five-time points (see Supplementary Information Table S3), and these five networks all belong to phase **I**. Fig. 3 shows the complementary cumulative distribution function, probability distribution function and degree-dependent clustering coefficient versus node degrees. Examining these characteristics, they are self-similar. The FFS analysis is performed along the GR flow, and the results

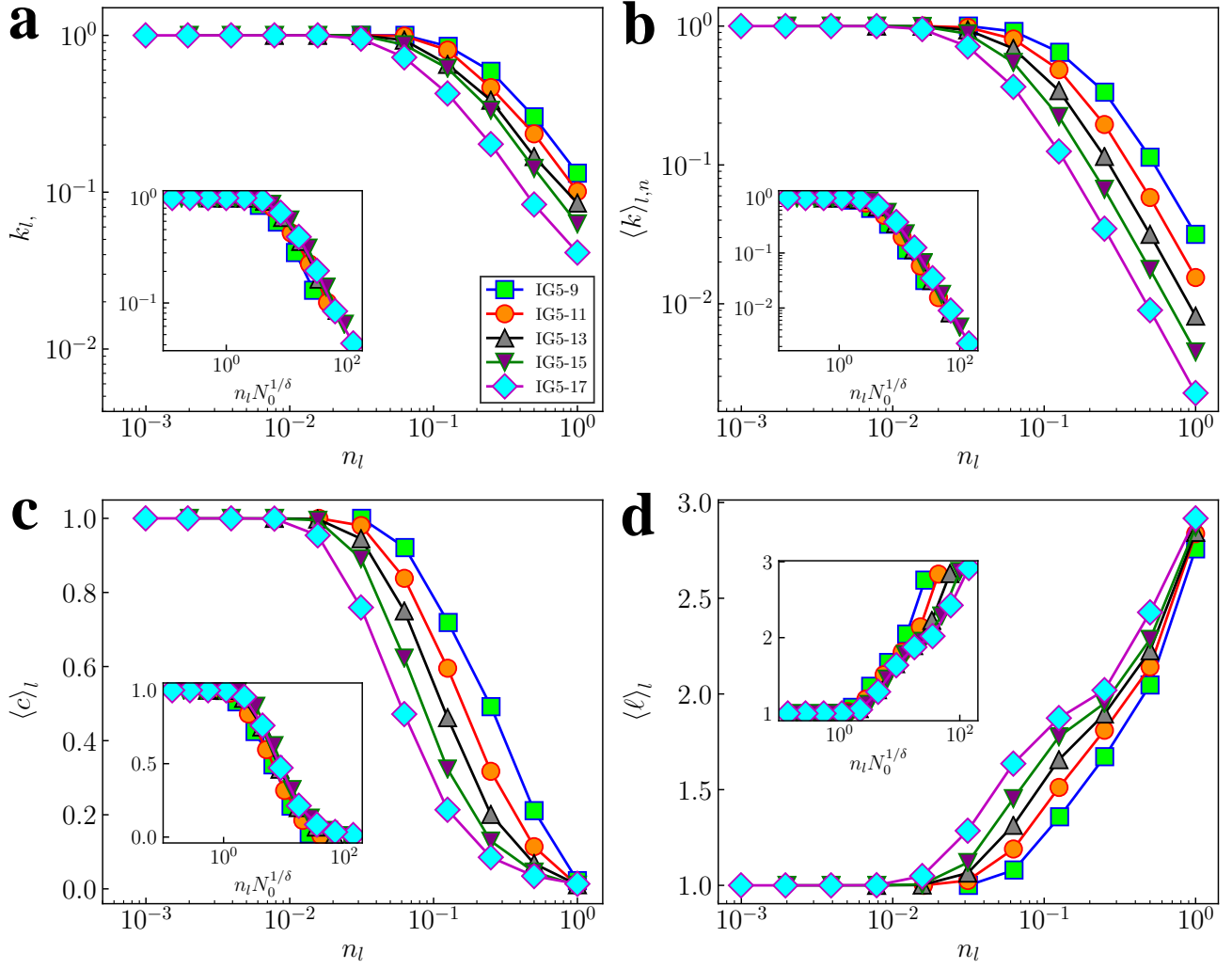


Figure 4: FSS analysis of IG5 evolutionary networks' topological observables along the GR flow. The main figures show each observable as a function of the variable n_l in the process of GR transformation, and the inset shows their scaling functions related to the variable $n_l N_0^{1/\delta}$. These networks belong to phase **I**, and the scaling exponent corresponding to four observables is $\delta = 2 \pm 0.1$.

suggest that there is a phenomenon similar to that of synthetic networks, that is, the curves of each observable almost overlap under the scaling function with $n_l N_0^{1/\delta}$ as the variable, and the exponent $\delta \approx 2$ (see Fig. 4 and Fig. 5). The other nine types of evolutionary networks produced similar results (see Supplementary Information Figs. S12-S38), further confirming that the exponent δ can be used as a effective measure for dividing small-world and non-small-world networks.

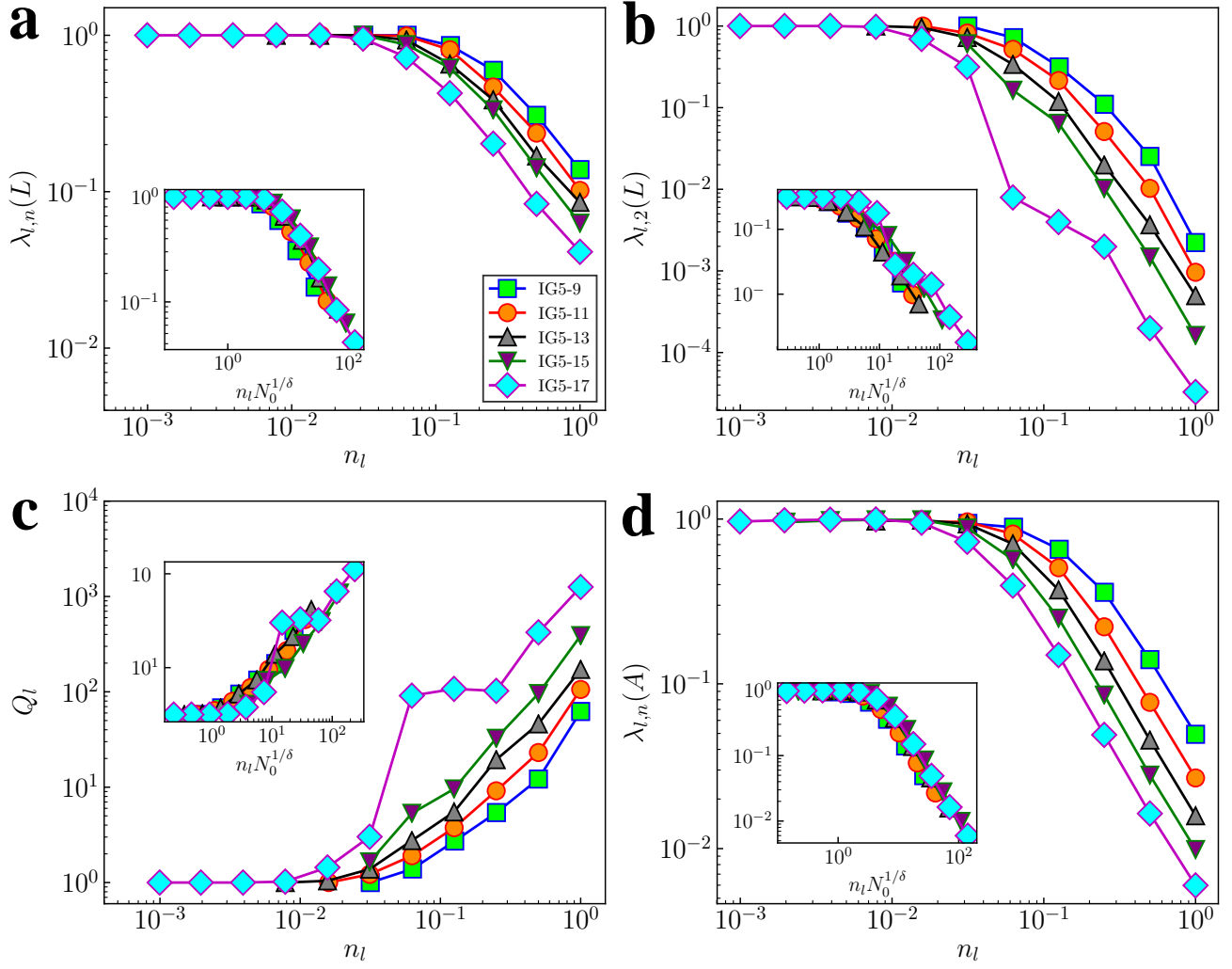


Figure 5: FSS analysis of IG5 evolutionary networks' dynamic observables along the GR flow. The main figures show each observable as a function of the variable n_l in the process of GR transformation, and the inset shows their scaling functions related to the variable $n_l N_0^{1/\delta}$. The scaling exponent corresponding to four observables is $\delta = 2 \pm 0.1$.

Discussion

In conclusion, the scaling behaviors of structural and dynamical observables of \mathbb{S}^1 synthetic and real evolutionary networks have been systematically investigated along the GR flows. According to the structural properties of the \mathbb{S}^1 model, the network evolutionary phase can be divided into three regions. Some networks with different structural parameters are generated in each region, with finite-size scaling analysis on their structural and dynamical observables. The results show that these observables can be characterized by a certain scaling function with $n_l N_0^{1/\delta}$ as the variable. More importantly, the critical exponent δ is found to be independent of these observables but dependant only on the small-world properties of the network. More

precisely, networks located in the small-world phase region all have exponent $\delta = 2$, while those located in the non-small-world phase region and in their critical regions all have $\delta = 1$. This implies that the \mathbb{S}^1 model can be divided into two universal types according to the value of the exponent δ .

Inspired by the findings on model \mathbb{S}^1 , some real evolutionary network systems are considered, typically in the small-world phase, which also follows the finite-size scaling found in model \mathbb{S}^1 . Specifically, for each system, there are different sizes at different time points. By embedding these networks of different sizes into the \mathbb{S}^1 network, it was found that they all approximate the same phase on the (ν, σ) plane, and these networks are self-similar. Thus, this investigation continues to study the scaling laws of some real evolutionary systems in the same way as the synthetic networks. The findings further suggest that the \mathbb{S}^1 model can provide more evidence for predicting the structural and dynamical behavior of those real networks. On the other hand, the results of this paper can provide some guidance for studying the structural and functional characteristics of large-scale networks. For instance, for an evolutionary network, often with a relatively small initial size, will eventually evolve to a large-scale system, so that it is difficult to obtain its structural and functional characteristics via computer simulation. While the scaling law found in this paper makes it possible to predict the characteristics of large-scale networks from small-size networks. Furthermore, the new results also show that the GR transformation may lead to significant changes of some properties of the network, which can be captured by the scaling function under the finite-size scaling analysis.

References

- [1] S. Boccaletti, V. Latora, Y. Moreno, M. Chavez, and D.-U. Hwang. Complex networks: Structure and dynamics. *Phys. Rep.*, 424:175–308, 2006.
- [2] A.-L. Barabási. *Network Science*. Cambridge University Press, Cambridge, 2016.
- [3] D. J. Watts and S. H. Strogatz. Collective dynamics of ‘small-world’ networks. *Nature*, 393:440–442, 1998.
- [4] A.-L. Barabási and R. Albert. Emergence of scaling in random networks. *Science*, 286:509–512, 1999.
- [5] A. Arenas, A. Díaz-Guilera, J. Kurths, Y. Moreno, and C. Zhou. Synchronization in complex networks. *Phys. Rep.*, 469:93–153, 2008.
- [6] V. Nicosia, M. Valencia, M. Chavez, A. Díaz-Guilera, and V. Latora. Remote synchronization reveals network symmetries and functional modules. *Phys. Rev. Lett.*, 110:174102, 2013.
- [7] Y. Y. Liu, J. J. Slotine, and A.-L. Barabási. Controllability of complex networks. *Nature*, 473:167–173, 2011.
- [8] Y. Y. Liu, J. J. Slotine, and A.-L. Barabási. Observability of complex systems. *Proc. Natl. Acad. Sci. U.S.A.*, 110:2460–2465, 2013.

- [9] V. Colizza, R. Pastor-Satorras, and A. Vespignani. Reaction-diffusion processes and metapopulation models in heterogeneous networks. *Nat. Phys.*, 3:276–282, 2007.
- [10] J. M. Kleinberg. Navigation in a small world. *Nature*, 406:845, 2000.
- [11] E. López, S. V. Buldyrev, S. Havlin, and H. E. Stanley. Anomalous transport in scale-free networks. *Phys. Rev. Lett.*, 94:248701, 2005.
- [12] G. Li, S. D. S. Reis, A. A. Moreira, S. Havlin, H. E. Stanley, and J. S. Andrade. Towards design principles for optimal transport networks. *Phys. Rev. Lett.*, 104:018701, 2010.
- [13] M. E. J. Newman and D. J. Watts. Renormalization group analysis of the small-world network model. *Phys. Lett. A*, 263:341, 1999.
- [14] L. P. Kadanoff. *Statistical Physics: Static, Dynamics and Renormalization*. World Scientific, Singapore, 2000.
- [15] B. J. Kim. Geographical coarse graining of complex networks. *Phys. Rev. Lett.*, 93:168701, 2004.
- [16] D. Gfeller and P. De Los Rios. Spectral coarse graining of complex networks. *Phys. Rev. Lett.*, 99:038701, 2007.
- [17] C. Song, S. Havlin, and H. A. Makse. Self-similarity of complex networks. *Nature*, 433:392–395, 2005.
- [18] C. Song, S. Havlin, and H. A. Makse. Origins of fractality in the growth of complex networks. *Nat. Phys.*, 2:275–281, 2006.
- [19] C. Song, L. K. Gallos, S. Havlin, and H. A. Makse. How to calculate the fractal dimension of a complex network: the box covering algorithm. *J. Stat. Mech.*, page P03006, 2007.
- [20] K. I. Goh, G. Salvi, B. Kahng, and D. Kim. Skeleton and fractal scaling in complex networks. *Phys. Rev. Lett.*, 96:018701, 2006.
- [21] J. S. Kim, K. I. Goh, B. Kahng, and D. Kim. Fractality and self-similarity in scale-free networks. *New. J. Phys.*, 9:177, 2007.
- [22] J. S. Kim, K. I. Goh, G. Salvi, E. Oh, B. Kahng, and D. Kim. Fractality in complex networks: Critical and supercritical skeletons. *Phys. Rev. E*, 75:016110, 2007.
- [23] F. Radicchi, J. J. Ramasco, A. Barrat, and S. Fortunato. Complex networks renormalization: Flows and fixed points. *Phys. Rev. Lett.*, 101:148701, 2008.
- [24] F. Radicchi, A. Barrat, S. Fortunato, and J. J. Ramasco. Renormalization flows in complex networks. *Phys. Rev. E*, 79:026104, 2009.
- [25] H. D. Rozenfeld, C. Song, and H. A. Makse. Small-world to fractal transition in complex networks: A renormalization group approach. *Phys. Rev. Lett.*, 104:025701, 2010.

- [26] G. García-Pérez, M. Boguñá, and M. Á. Serrano. Multiscale unfolding of real networks by geometric renormalization. *Nat. Phys.*, 14:583–589, 2018.
- [27] M. Á. Serrano, D. Krioukov, and M. Boguñá. Self-similarity of complex networks and hidden metric spaces. *Phys. Rev. Lett.*, 100:078701, 2008.
- [28] D. Krioukov, F. Papadopoulos, A. Vahdat, and M. Boguñá. Curvature and temperature of complex networks. *Phys. Rev. E*, 80:035101(R), 2009.
- [29] D. Krioukov, F. Papadopoulos, M. Kitsak, A. Vahdat, and M. Boguñá. Hyperbolic geometry of complex networks. *Phys. Rev. E*, 82:036106, 2010.
- [30] F. Papadopoulos, M. Kitsak, M. Á. Serrano, M. Boguñá, and D. Krioukov. Popularity versus similarity in growing networks. *Nature*, 489:537–540, 2012.
- [31] M. Boguñá, F. Papadopoulos, and D. Krioukov. Sustaining the internet with hyperbolic mapping. *Nature Communications*, 1:62, 2010.
- [32] A. Allard, M. Á. Serrano, G. García-Pérez, and M. Boguñá. The geometric nature of weights in real complex networks. *Nature Communications*, 8:14103, 2017.
- [33] A. Brouwer. *Spectra of Graphs*. Springer, New York, 2012.
- [34] T. Nishikawa, J. Sun, and A. E. Motter. Sensitive dependence of optimal network dynamics on network structure. *Phys. Rev. X*, 7:041044, 2017.
- [35] M. Barahona and L. M. Pecora. Synchronization in small-world systems. *Phys. Rev. Lett.*, 89:054101, 2002.
- [36] T. Nishikawa, A. E. Motter, Y.-C. Lai, and F. C. Hoppensteadt. Heterogeneity in oscillator networks: Are smaller worlds easier to synchronize. *Phys. Rev. Lett.*, 91:014101, 2003.
- [37] L. Donetti, P. I. Hurtado, and M. A. Muñoz. Entangled networks, synchronization, and optimal network topology. *Phys. Rev. Lett.*, 95:188701, 2005.
- [38] T. Nishikawa and A. E. Motter. Synchronization is optimal in non-diagonalizable networks. *Phys. Rev. E*, 73:065106(R), 2006.
- [39] T. Nishikawa and A. E. Motter. Maximum performance at minimum cost in network synchronization. *Physica D*, 224D:77–89, 2006.
- [40] M. Brede. Optimal synchronization in space. *Phys. Rev. E*, 81:025202(R), 2010.
- [41] D. H. Shi, G. Chen, W. W. K. Thong, and X. Y. Yan. Searching for optimal network topology with best possible synchronizability. *IEEE Circ. Sys. Mag.*, 13:66–75, 2013.
- [42] C. Castellano and R. Pastor-Satorras. Relating topological determinants of complex networks to their spectral properties: Structural and dynamical effects. *Phys. Rev. X*, 7:041024, 2017.

- [43] J. G. Restrepo, E. Ott, and B. R. Hunt. Onset of synchronization in large networks of coupled oscillators. *Phys. Rev. E*, 71:036151, 2005.
- [44] R. A. Rossi and N. K. Ahmed. The network data repository with interactive graph analytics and visualization. *Proc. of 29th AAAI Conference on Artificial Intelligence*, 2015.
- [45] J. Leskovec, J. Kleinberg, and C. Faloutsos. Graph evolution: densification and shrinking diameters. *ACM Trans. Knowl. Discov. Data (ACM TKDD)*, page 1(1), ACM, 2007.
- [46] M. Ripeanu, I. Foster, and A. Iamnitchi. Mapping the gnutella network: properties of large-scale peer-to-peer systems and implications for system design. *IEEE Internet Comput.*, 2002.
- [47] J. Leskovec, J. Kleinberg, and C. Faloutsos. Graphs over time: densification laws, shrinking diameters and possible explanations. In *Proc. 17th ACM SIGKDD International Conference on Knowledge Discovery and Data Mining*, pages 177–187, ACM, 2005.
- [48] M. E. J. Newman. The structure of scientific collaboration networks. *Proc. Natl. Acad. Sci. USA*, 98:404–409, 2001.
- [49] G. García-Pérez, A. Allard, M. Á. Serrano, and M. Boguñá. Mercator: uncovering faithful hyperbolic embeddings of complex networks. *New J. Phys.*, 21:123033, 2019.

Acknowledgments

We sincerely acknowledge G. García-Pérez, M. Boguñá, and M. Á. Serrano for sharing the codes of the geometric renormalization of general networks, and their suggestions have played an important role in improving the quality of the paper. This work was supported by the National Natural Science Foundation of China under Grant Nos. 61991412 and 61873318, the Frontier Research Funds of Applied Foundation of Wuhan under Grant No. 2019010701011421, and the Program for HUST Academic Frontier Youth Team under Grant No. 2018QYTD07.

Author contributions

All authors conceived the work, analyzed results, and wrote the manuscript. D. Chen wrote Python implementations.

Competing interests

The authors declare that they have no competing interests.

Data and materials availability

The data that support the plots within this paper and other findings of this study are available from the corresponding author upon request.

Supplementary Information for “Finite-size scaling of geometric renormalization flows in complex networks”

Dan Chen,¹ Housheng Su,^{1,*} Xiaofan Wang,² Gui-Jun Pan,³ and Guanrong Chen⁴

¹*School of Artificial Intelligence and Automation,
Image Processing and Intelligent Control Key Laboratory of Education Ministry of China,
Huazhong University of Science and Technology, Wuhan 430074, China*

²*Department of Automation, Shanghai University, Shanghai 200072, China*

³*Faculty of Physics and Electronic Science, Hubei University, Wuhan 430062, China*

⁴*Department of Electrical Engineering, City University of Hong Kong, Hong Kong, China*

* shs@hust.edu.cn

In this file of Supplementary Information, we first review the generation process of the \mathbb{S}^1 geometric model, and then show the average degree behavior of the \mathbb{S}^1 network model in different parameter regions through the geometric renormalization (GR) transformation process. Finally, we perform FSS analysis on eight observables of \mathbb{S}^1 type of synthetic networks (in regions II, III, and its critical region) and real evolutionary networks, respectively.

I. THE \mathbb{S}^1 GEOMETRIC MODEL

A network can be embedded into a hidden metric space [1–3] based on the distance between nodes in the space, where the edges between nodes are dominated by popularity and similarity dimensions [4]. Precisely, popularity is directly related to the degrees of the nodes, while similarity is the sum of many other attributes that can regulate the possibility of interaction between nodes [5]. The model generated by these two mechanisms can clearly explain some universal properties of real networks, such as the structural complexity, evolutionary mechanism, and dynamical behaviors.

Consider a simple one-dimensional \mathbb{S}^1 geometric model [1], in which N nodes are placed on the circle of radius R . Each node i is dominated by two latent variables, one is the angle θ_i of the node i in the circle coordinates, used as the similarity measure, and the other is the hidden degree value κ_i , which is associated with the prevalence of the node, and is proportional to the desired degree of the node in the network. In the model, θ_i is uniformly randomly taken from the interval $[0, 2\pi)$, and the value of κ_i satisfies the probability density function $\phi(\kappa) = (1 - \nu)\kappa^{-\nu} / (\kappa_c^{1-\nu} - \kappa_0^{1-\nu}) \sim \kappa^{-\nu}$, $\kappa_0 \leq \kappa \leq \kappa_c$, $\kappa_0 = \langle k \rangle (\nu - 2) / (\nu - 1)$, $\kappa_c = \kappa_0 N^{1/(\nu-1)}$, with $\nu > 2$. Therefore, for nodes with large degrees, the observed degree distribution is approximately the same as $\phi(\kappa)$, i.e., $\Phi(k) \sim k^{-\nu}$. The radius R of the circle is proportional to the total number of nodes, N . For simplicity, set $N = 2\pi R$, which ensures that the average density of the nodes on the circle is equal to 1. The probability of connecting two nodes in hidden coordinates (θ_i, κ_i) and (θ_j, κ_j) on the circle is given by

$$p_{ij} = \frac{1}{1 + \psi_{ij}^\sigma} = \frac{1}{1 + \left[\frac{d(\theta_i, \theta_j)}{\mu \kappa_i \kappa_j} \right]^\sigma}, \quad (\text{S1})$$

where $d(\theta_i, \theta_j) = R\Delta\theta_{ij}$ is the geodesic distance between nodes i and j on the circle, and $\Delta\theta_{ij} = \pi - |\pi - |\theta_i - \theta_j||$. Equation (S1) indicates that the connection probability between nodes increases with the product of the hidden degrees, but decreases with the increase of their distance along the circle [5]. The parameter μ controls the observed average degree of the network, and the parameter σ controls the average clustering coefficient of the network, such that the larger the value is and the smaller the effective distance is, the more advantageous it is to the increase of the average clustering in the network [1].

II. AVERAGE DEGREE BEHAVIORS IN GR FLOWS OF THE \mathbb{S}^1 MODEL

In [5], a GR framework for complex networks is defined based on a hidden metric space [1–4]. This GR transformation has a good characteristic that it can well predict the average degree behavior of a large-scale network in the GR flow process. Taking the \mathbb{S}^1 model for example, in [5], the average degree is shown to approximate satisfactorily an exponential relation along the GR flow, as

$$\langle k \rangle_l = s^\alpha \langle k \rangle_{l-1}, \quad (\text{S2})$$

where the exponent α depends on the parameters ν and σ , with

$$\alpha = \begin{cases} \frac{2}{\nu-1} - 1, & 0 < \nu - 1 \leq \sigma, \\ \frac{2}{\sigma} - 1, & \sigma \leq \nu - 1 < 2\sigma. \end{cases} \quad (\text{S3})$$

According to Eq. (S3), the \mathbb{S}^1 model can be roughly divided into three regions [5]:

I: $\nu < 3$ or $\sigma < 2$ and $\alpha > 0$, which corresponds to the small-world phase. Along the direction of the GR flow, the network eventually approaches a highly connected graph. That is, in this region, the average degree of the network increases gradually along the GR flow (see the blue straight solid-line in Fig. S1).

I to II: $\nu = 3$ and $\sigma \geq 2$ or $\sigma = 2$ and $\nu \geq 3$, namely the network is at the critical region from the small-world phase to the non-small-world phase. According to Eq. (S3), when the value of (ν, σ) is on the boundary line, $\alpha = 0$, the average degree of the network remains almost unchanged along the GR flow (see the red straight solid-line in Fig. S1).

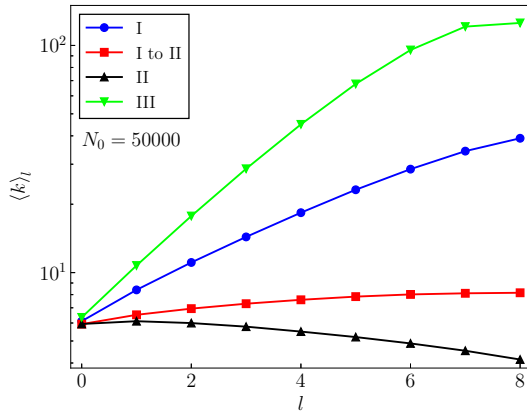


FIG. S1. The average degree $\langle k \rangle_l$ as a function of l for renormalized networks. Each curve represents the variation of the average degree of a particular network in the corresponding region along the GR flow. In region I, $(\nu, \sigma) = (2.5, 1.5)$. At the edge of the transition between regions I and II, $(\nu, \sigma) = (3.0, 2.5)$. In region II, $(\nu, \sigma) = (3.5, 2.5)$. In region III, $(\nu, \sigma) = (4.0, 1.1)$. The average hidden degree $\langle \kappa \rangle_0 \approx 6$ and the expected average degree $\langle k \rangle_0 \approx 6$ for all initial networks. The sizes of the initial networks are $N_0 = 50000$. All the results are averaged over 10 independent realizations.

II: $\nu > 3$ and $\sigma > 2$, namely the network is located in the non-small-world phase, the exponent $\alpha < 0$, along the direction of the GR flow, the renormalized network becomes more and more sparse and finally tends to a one-dimensional ring structure (see the black straight solid-line in Fig. S1); as the renormalization process proceeds, the network eventually lose the small-world property.

III: $2\sigma < \nu - 1$, where the network becomes increasingly homogeneous as $s \rightarrow \infty$ (or $l \rightarrow \infty$), consequently the network degree distribution lose its scale-freeness along the GR flow. From simulations, it was found that the average degree of the renormalized layer has a similar behavior with Eq. (S2) (see the green straight solid-line in Fig. S1), i.e., $\langle k \rangle_l = s^\alpha \langle k \rangle_{l-1}$.

Fig. S1 shows the dependence of the average degree $\langle k \rangle_l$ of a particular network on the renormalized layer l within each region. Within regions I and III, $\langle k \rangle_l$ approximates an exponential growth. At the edge of the transition between regions I and II, the average degree $\langle k \rangle_l$ presents a tendency of slow increase with the increase of l , which gradually becomes saturated. Within region II, the average degree $\langle k \rangle_l$ approximates an exponential decay. The structure of the renormalized network is similar to a ring as a fixed point. When the initial network size is large enough, the above phenomena show better consistency with Eq. (S2). Moreover, Fig. S1 further shows that the value of the parameter α can be used as a measure to distinguish between small-world and non-small-world network. That is, when $\alpha > 0$, the network in phase I or III, belongs to a small-world network; when $\alpha \leq 0$, the network in phase II or in their critical region, belongs to the non-small-world network.

III. FSS ANALYSIS OF NETWORK OBSERVABLES

A. Synthetic networks

FSS is performed, along the direction of a GR flow, on eight observables of networks in their critical region (at the edge of regions I and II), region II, and region III, respectively. Specifically, the dependence of these observables on n_l is investigated for each layer of the renormalized network. The results indicate that these observables can be represented by scaling functions with $n_l N_0^{1/\delta}$ as the variable.

Consider the \mathbb{S}^1 network under the different sets of parameters (ν, σ) in the above three regions. It is worth noting that, for networks of different sizes with a specific set of parameters, the exponent δ is approximately equal to the same value for all the eight observables in the process of GR transformation. Table S1 shows the detailed results.

Fig. S2 shows the dependence of $k_{l,\max}$, $\langle k \rangle_{l,n}$, $\langle c \rangle_l$ and $\langle \ell \rangle_l$ on n_l . At the edge between regions I and II, the average degree almost remains constant along the GR flow, with $(\nu, \sigma) = (3.0, 2.5)$, the exponent $\delta \approx 1$ (see the inset of Fig. S2). And in region II (non-small-world phase) with $(\nu, \sigma) = (3.5, 2.5)$, the scaling exponent $\delta \approx 1$ (see Fig. S4). While in region III, Fig. S1 shows that the average degree of the network increases gradually along the GR flow. The results in [5] show that the network in this region has a homogeneous degree distribution. Here, the results further

Region	(ν, σ)	δ
I	(2.1,1.1)	2 ± 0.1
	(2.1,1.5)	2 ± 0.1
	(2.5,1.5)	2 ± 0.1
	(3.0,1.1)	2 ± 0.1
	(3.5,1.5)	2 ± 0.05
I to II	(3.0,2.5)	1 ± 0.05
	(3.5,2.0)	1 ± 0.05
II	(3.5,2.5)	1 ± 0.05
	(4.0,3.0)	1 ± 0.05
III	(3.5,1.1)	2 ± 0.05
	(4.0,1.1)	2 ± 0.05

TABLE S1. In every region, consider the S^1 network with several different sets of parameters (ν, σ) . For each set of parameters, select four different initial network sizes, $N_0 = 5000, 10000, 20000$ and 50000 , respectively. The average hidden degree $\langle \kappa \rangle_0 \approx 6$ and the expected average degree $\langle k \rangle_0 \approx 6$ for all initial networks. In the process of GR transformation, each observable can be characterized by a scaling function with $n_l N_0^{l/\delta}$ as the variable. For every observable, the results show that the function curves of different sizes largely overlap. Values of the exponent δ corresponding to all observables are almost identical. All numerical results are averaged over 10 independent realizations.

show that networks in this region also have small-world characteristics. With $(\nu, \sigma) = (4.0, 1.1)$, the exponent $\delta \approx 2$, as shown in the inset of Fig. S6.

Combined with the conclusions in the main text, the results here show that, when the network is in the small-world phase (regions I and III), the average degree of the renormalized network increases gradually along the GR flow, i.e., the parameter $\alpha > 0$ in Eq. (S3), and the exponent $\delta \approx 2$. When the network is in the non-small-world phase and in their critical region, the parameter $\alpha \leq 0$, and the exponent $\delta \approx 1$. Therefore, the S^1 model can be roughly divided into two universal classes according to the critical exponent δ , i.e., in small-world or non-small-world phase, respectively.

Note that, when the network is in region I or III, $k_{l,\max}$ and $\langle k \rangle_{l,n}$ can converge to the saturated value 1 at a faster speed after a finite steps of GR iterations; that is, the maximum degree and the average degree of the renormalized network G_l satisfy $K_l = N_l - 1$ and $\langle k \rangle_l = N_l - 1$, respectively.

The average clustering coefficient increases gradually along the GR flow and eventually reaches the maximum value 1, which further indicates that the network in these two regions takes the highly connected graph as the fixed point in the process of the GR flow. However, when the network is located at the edge between regions I and II or within region II, $k_{l,\max}$ and $\langle k \rangle_{l,n}$ are less than 1 after the same number of GR iterations. Particularly, this phenomenon is more obvious in region II. The average clustering coefficient shows a slight change along the GR flow, which means that the network in the non-small-world phase takes the one-dimensional ring structure as the fixed point in the process of GR iterations.

Region	(ν, σ)	$k_{l,\max}$	$\langle k \rangle_{l,n}$	$\lambda_{l,n}(L)$	$\lambda_{l,2}(L)$	Q_l	$\lambda_{l,n}(A)$
I	(2.5,1.5)	0.65	1.34	0.65	2.01	1.36	1.10
I to II	(3.0,2.5)	0.50	1.03	0.50	1.93	1.43	0.82
II	(3.5,2.5)	0.47	0.90	0.47	2.01	1.51	0.77
III	(4.0,1.1)	1.03	1.68	1.03	2.18	1.15	1.51

TABLE S2. By studying the dependence of six observables given in the main text depending on n_l (see Eqs. (3)–(6)), it was found that they all approximately obey power-law relations. Taking $k_{l,\max}$ for example, it approximately satisfies $k_{l,\max} \sim n_l^{-\beta}$. The values of the power-law exponent of each observable in the GR transformation process are listed here, for a specific initial network in each region. The size of the initial network is $N_0 = 50000$. The average hidden degree is $\langle \kappa \rangle_0 \approx 6$ and the expected average degree is $\langle k \rangle_0 \approx 6$. The exponent is obtained by fitting the average of 10 independent samples.

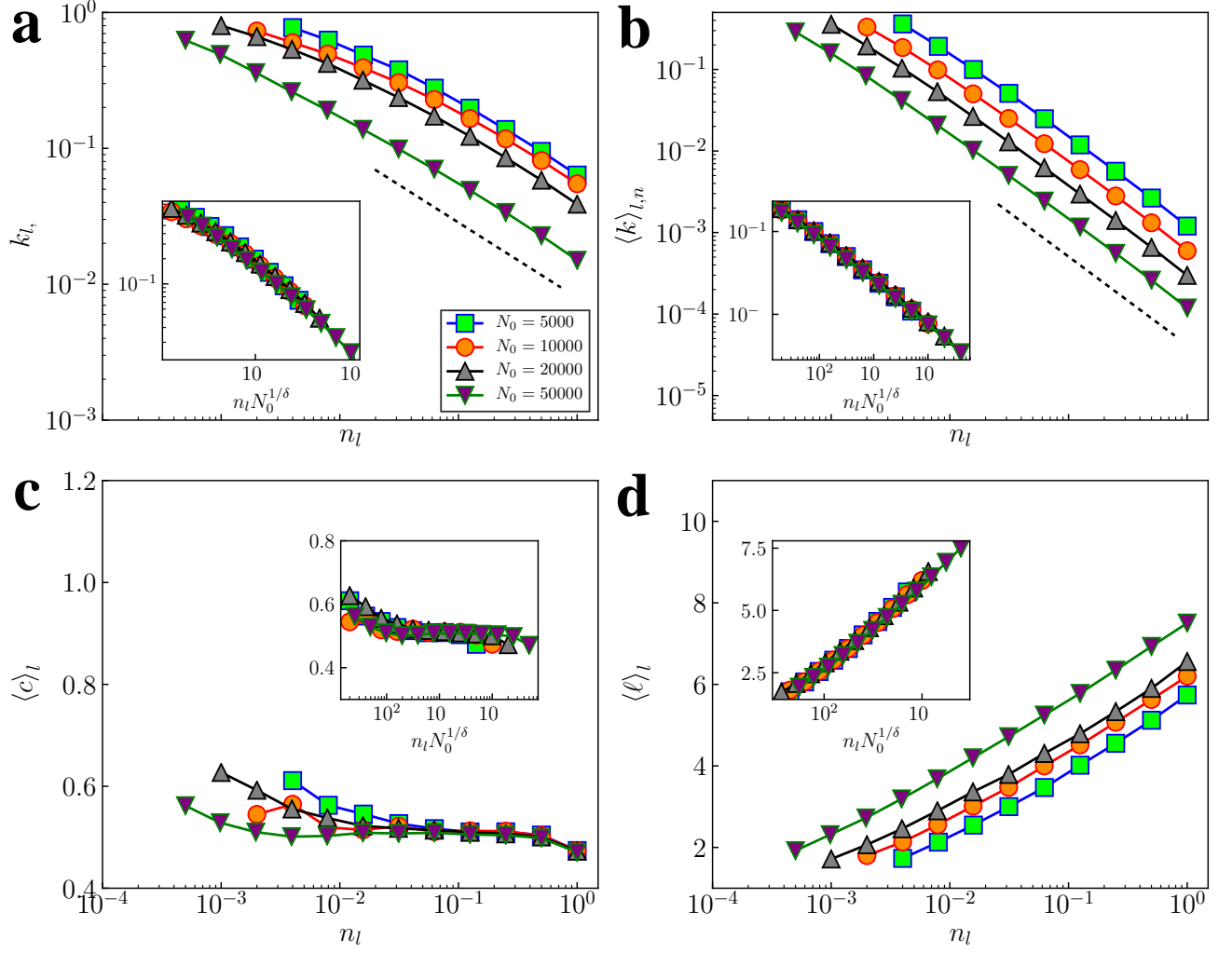
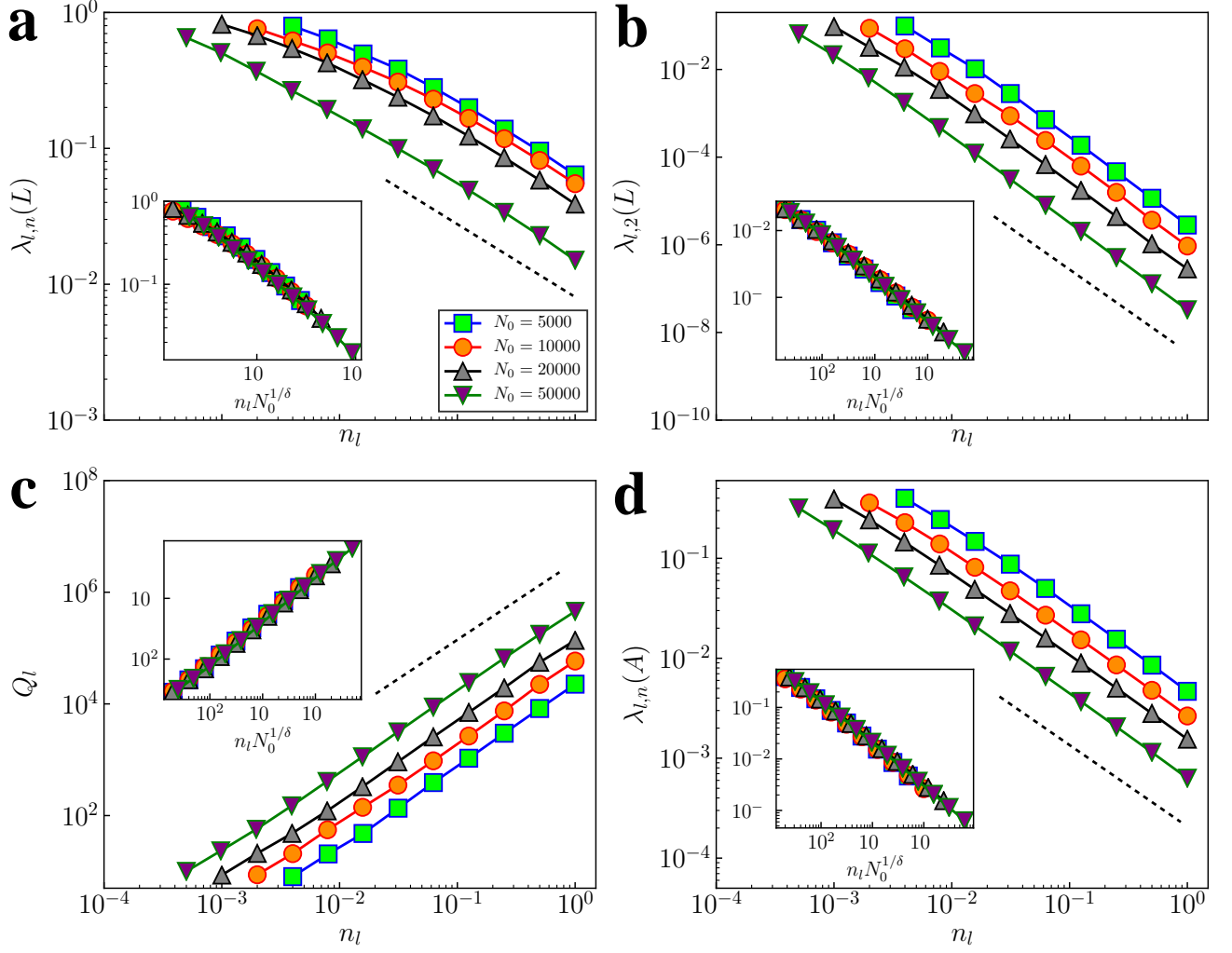


FIG. S2. FSS analysis of the \mathbb{S}^1 network topological observables along the GR flow. The main figures show every observable as a function of the variable n_l in the process of GR transformation, and the inset shows their scaling functions related to the variable $n_l N_0^{1/\delta}$. Key parameters of the \mathbb{S}^1 network are $\nu = 3.0$ and $\sigma = 2.5$, respectively. Values of the scaling exponent corresponding to four observables are all $\delta = 1 \pm 0.05$. For observables $k_{l,max}$ and $\langle k \rangle_{l,n}$, the black dashed-lines predict their power-law behaviors, where values of the power-law exponent are given in Table S2. The average hidden degree $\langle \kappa \rangle_0 \approx 6$ and the expected average degree $\langle k \rangle_0 \approx 6$ for all initial networks. All the results are averaged over 10 independent realizations.



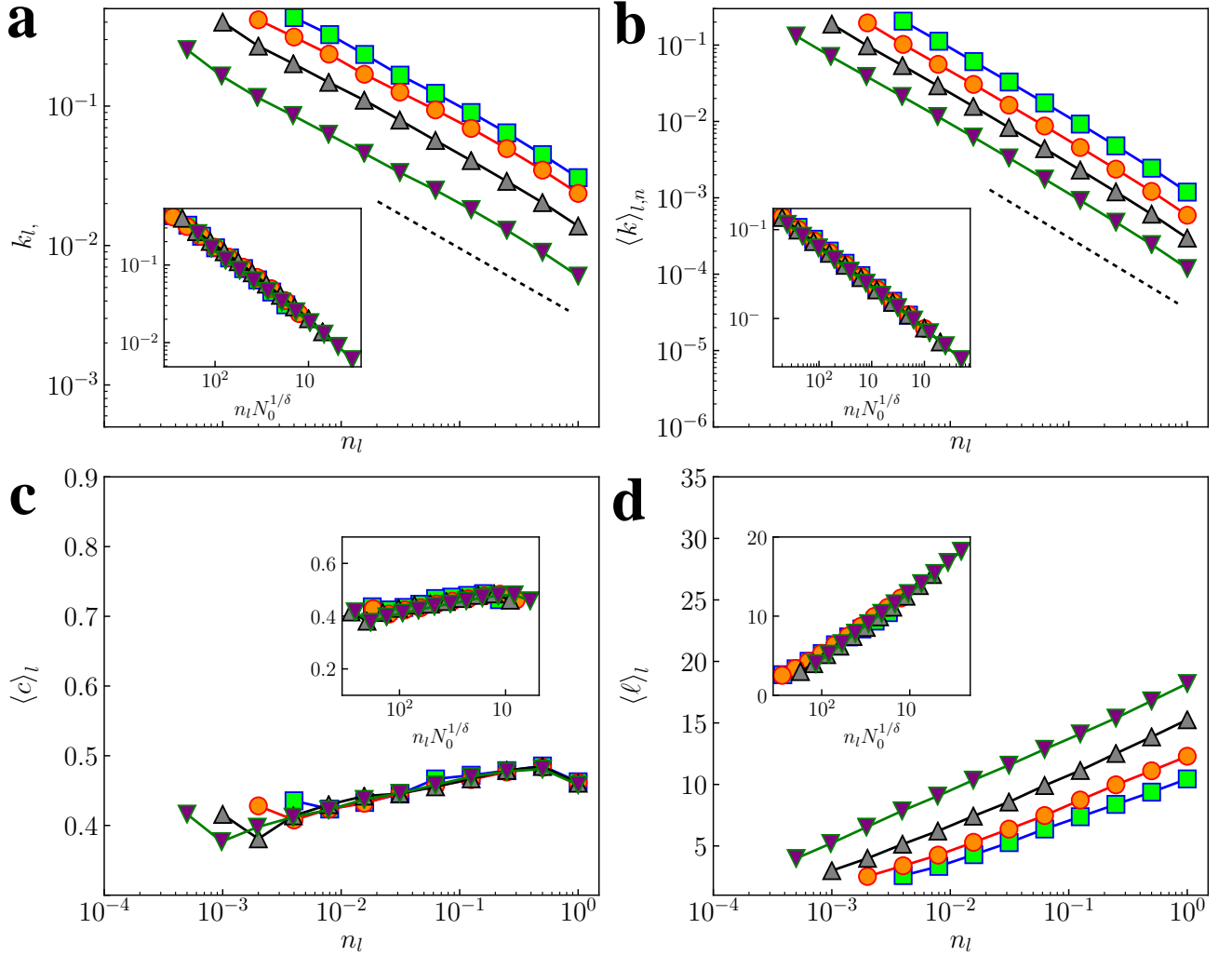


FIG. S4. FSS analysis of the \mathbb{S}^1 network topological observables along the GR flow. The main figures show every observable as a function of the variable n_l in the process of GR transformation, and the inset shows their scaling functions related to the variable $n_l N_0^{1/\delta}$. Key parameters of the \mathbb{S}^1 network are $\nu = 3.5$ and $\sigma = 2.5$, respectively. Values of the scaling exponent corresponding to four observables are all $\delta = 1 \pm 0.05$. For observables $k_{l,max}$ and $\langle k \rangle_{l,n}$, the black dashed-lines predict their power-law behaviors, where values of the power-law exponent are given in Table S2. The average hidden degree $\langle \kappa \rangle_0 \approx 6$ and the expected average degree $\langle k \rangle_0 \approx 6$ for all initial networks. All the results are averaged over 10 independent realizations.

Furthermore, compared with the network in region II, the network in region I or III has a smaller average shortest path-length $\langle \ell \rangle_l$, and $\langle \ell \rangle_l$ of the network in these two regions decreases faster than that in other regions along the GR flow, which eventually tends to the saturated value 1. Namely, the renormalized network finally evolves to a fully connected graph, which is completely consistent with the phenomenon revealed by the maximum degree and average degree of the network along the GR flow.

Finally, the dependence of $\lambda_{l,n}(L)$, $\lambda_{l,2}(L)$, Q_l and $\lambda_{l,n}(A)$ on n_l is investigated, with results shown in Fig. S3, Fig. S5, and Fig. S7. The inset shows the dependence of these observables on $n_l N_0^{1/\delta}$ for different sizes of networks, which is similar to the phenomenon presented in Fig. S2, Fig. S4, and Fig. S6, respectively, i.e., in critical region, $\delta \approx 1$, in region II, $\delta \approx 1$, and in region III, $\delta \approx 2$. The black dashed-line predicts the power-law behavior of each observable along the GR flow, the values of the power-law exponent are listed in Table S2. In addition, in regions I and III, all dynamical observables of the network converge to the stable values more quickly along the GR flow. For $\lambda_{l,n}(L)$, $\lambda_{l,2}(L)$, Q_l , and $\lambda_{l,n}(A)$, they all tend to the saturated value 1 in the end of the GR iterations. While in region II and in their critical region, $\lambda_{l,n}(L)$, $\lambda_{l,2}(L)$ and $\lambda_{l,n}(A)$ have smaller values, but Q_l has larger values. For $\lambda_{l,2}(L)$ and eigenvalue ratio Q_l , they are related to the diffusion time and the network synchronizability, respectively. These results indicate that the network located in regions I and III have a small diffusion time ($1/\Lambda_{l,2}(L)$) but a

strong synchronizability, which is completely consistent with the results in [5] (see Fig. S12 in the Supplementary Information in [5]). In fact, for higher-dimensional embedded synthetic networks \mathbb{S}^D ($D \geq 2$) [5], one may be able to get similar results to one-dimensional embedded networks \mathbb{S}^1 (see Figs. S8-S11).

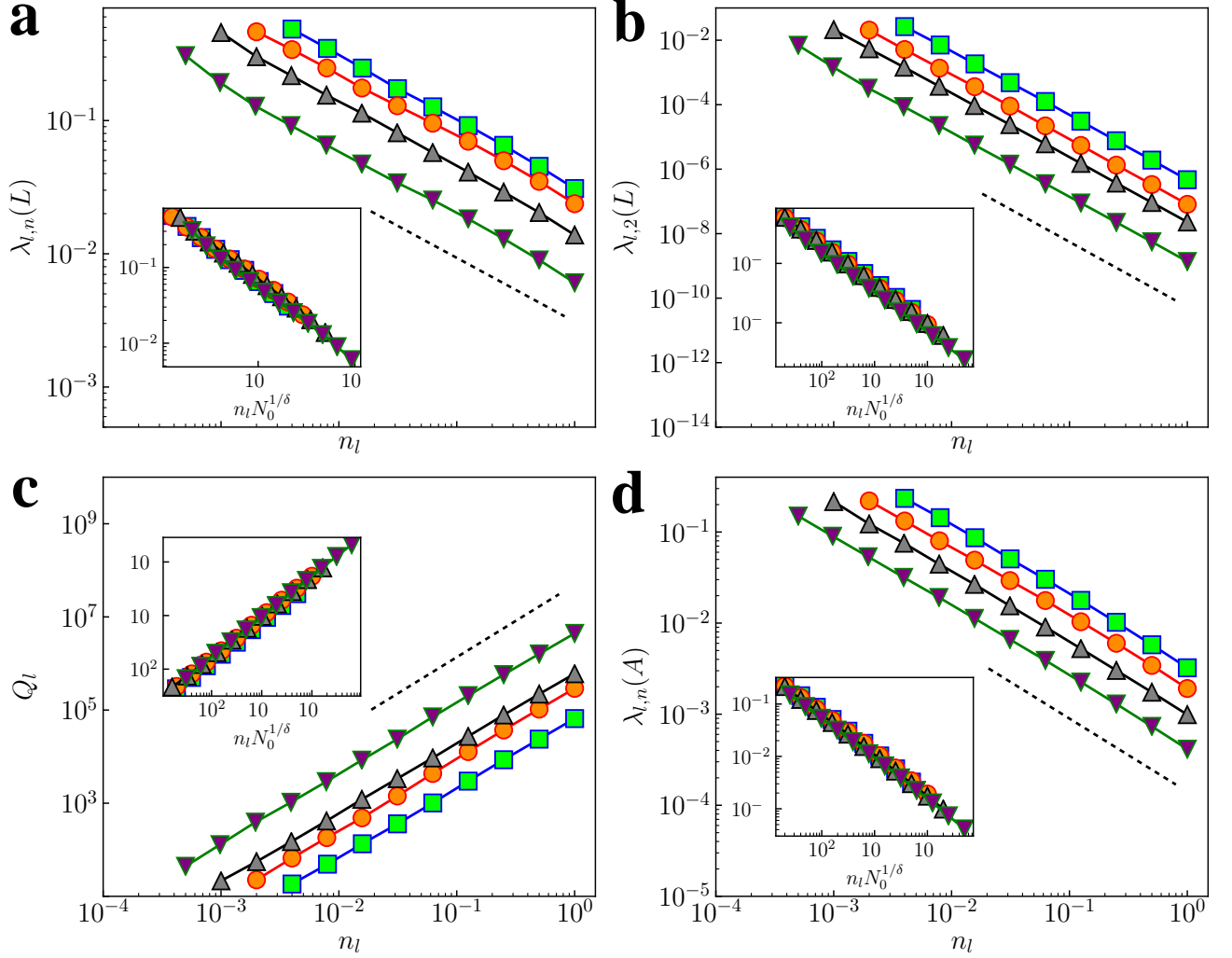


FIG. S5. FSS analysis of the \mathbb{S}^1 network dynamical observables along a GR flow. The main figures show each observable as a function of the variable n_l in the process of GR transformation. The inset shows their scaling functions related to the variable $n_l N_0^{1/\delta}$. Key parameters of the \mathbb{S}^1 network are $\nu = 3.5$ and $\sigma = 2.5$, respectively. The scaling exponent corresponding to four observables are all $\delta = 1 \pm 0.05$. For all observables, the black dashed-lines predict their power-law behaviors. The values of the power-law exponent are given in Table S2. The average hidden degree $\langle \kappa \rangle_0 \approx 6$ and the expected average degree $\langle k \rangle_0 \approx 6$ for all initial networks. All the results are averaged over 10 independent realizations.

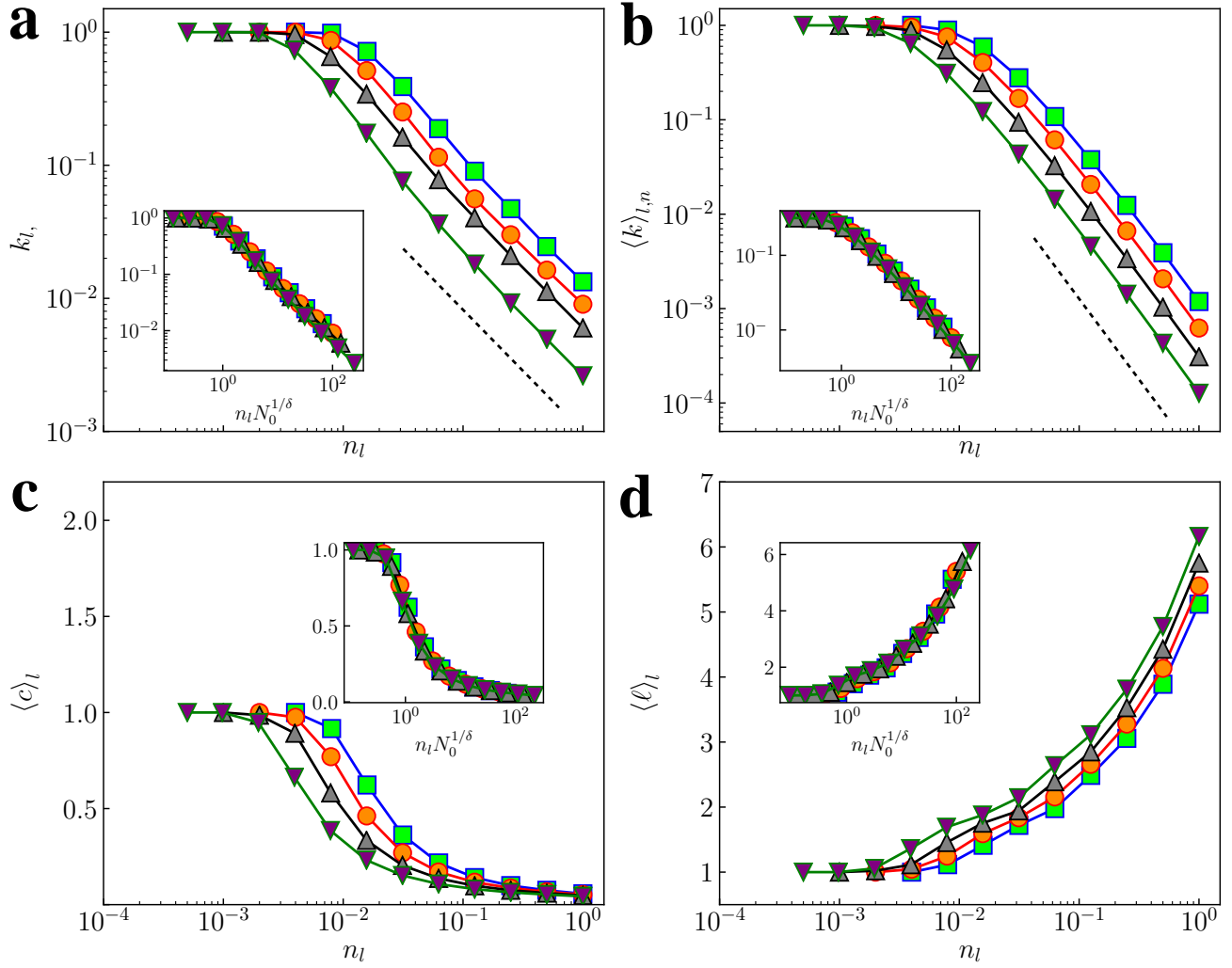


FIG. S6. FSS analysis of the \mathbb{S}^1 network topological observables along the GR flow. The main figures show every observable as a function of the variable n_l in the process of GR transformation, and the inset shows their scaling functions related to the variable $n_l N_0^{1/\delta}$. Key parameters of the \mathbb{S}^1 network are $\nu = 4.0$ and $\sigma = 1.1$, respectively. Values of the scaling exponent corresponding to four observables are all $\delta = 2 \pm 0.05$. For observables $k_{l,max}$ and $\langle k \rangle_{l,n}$, the black dashed-lines predict their power-law behaviors, where values of the power-law exponent are given in Table S2. The average hidden degree $\langle \kappa \rangle_0 \approx 6$ and the expected average degree $\langle k \rangle_0 \approx 6$ for all initial networks. All the results are averaged over 10 independent realizations.

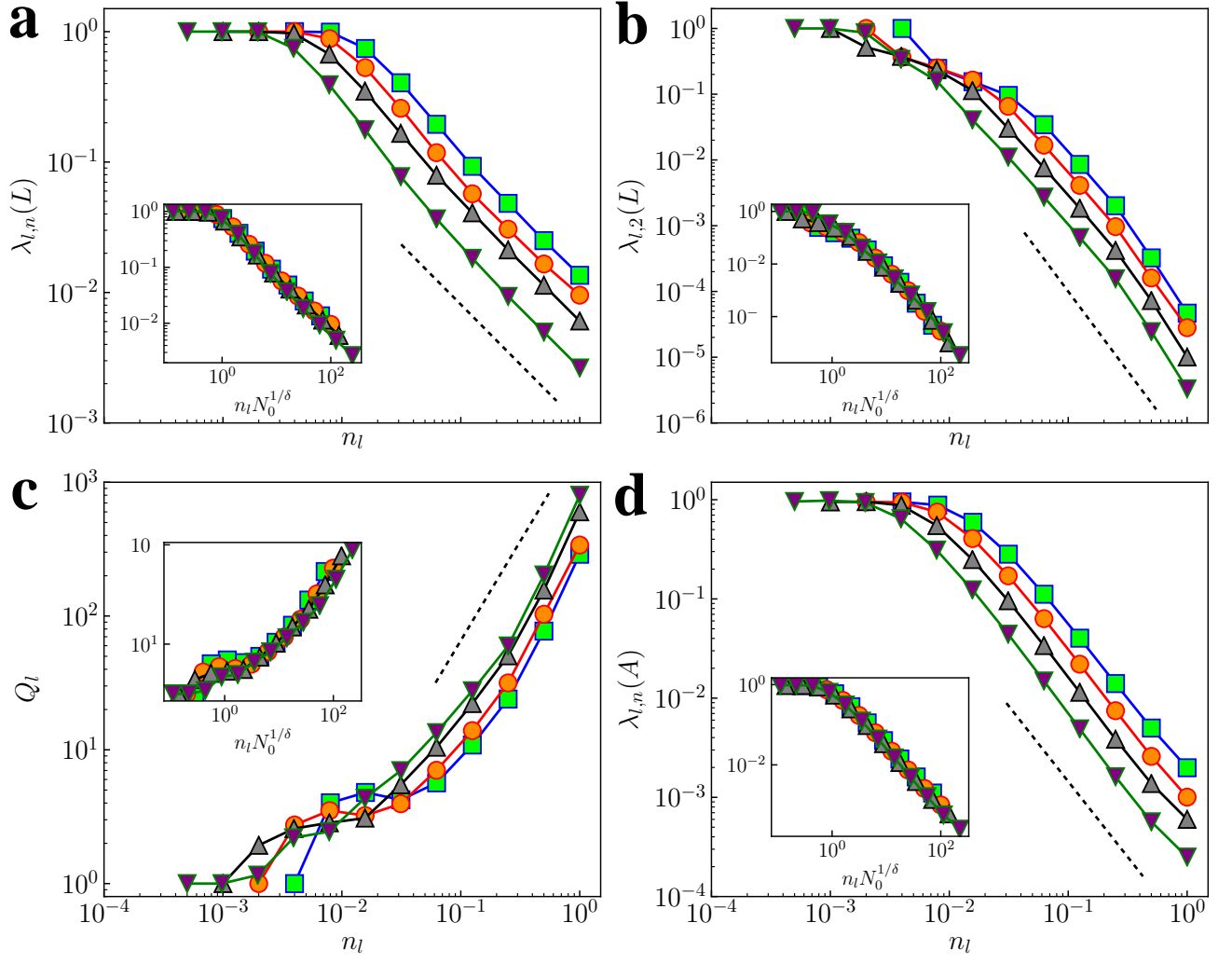


FIG. S7. FSS analysis of the \mathbb{S}^1 network dynamical observables along a GR flow. The main figures show each observable as a function of the variable n_l in the process of GR transformation. The inset shows their scaling functions related to the variable $n_l N_0^{1/\delta}$. Key parameters of the \mathbb{S}^1 network are $\nu = 4.0$ and $\sigma = 1.1$, respectively. The scaling exponent corresponding to four observables are all $\delta = 2 \pm 0.05$. For all observables, the black dashed-lines predict their power-law behaviors. The values of the power-law exponent are given in Table S2. The average hidden degree $\langle \kappa \rangle_0 \approx 6$ and the expected average degree $\langle k \rangle_0 \approx 6$ for all initial networks. All the results are averaged over 10 independent realizations.

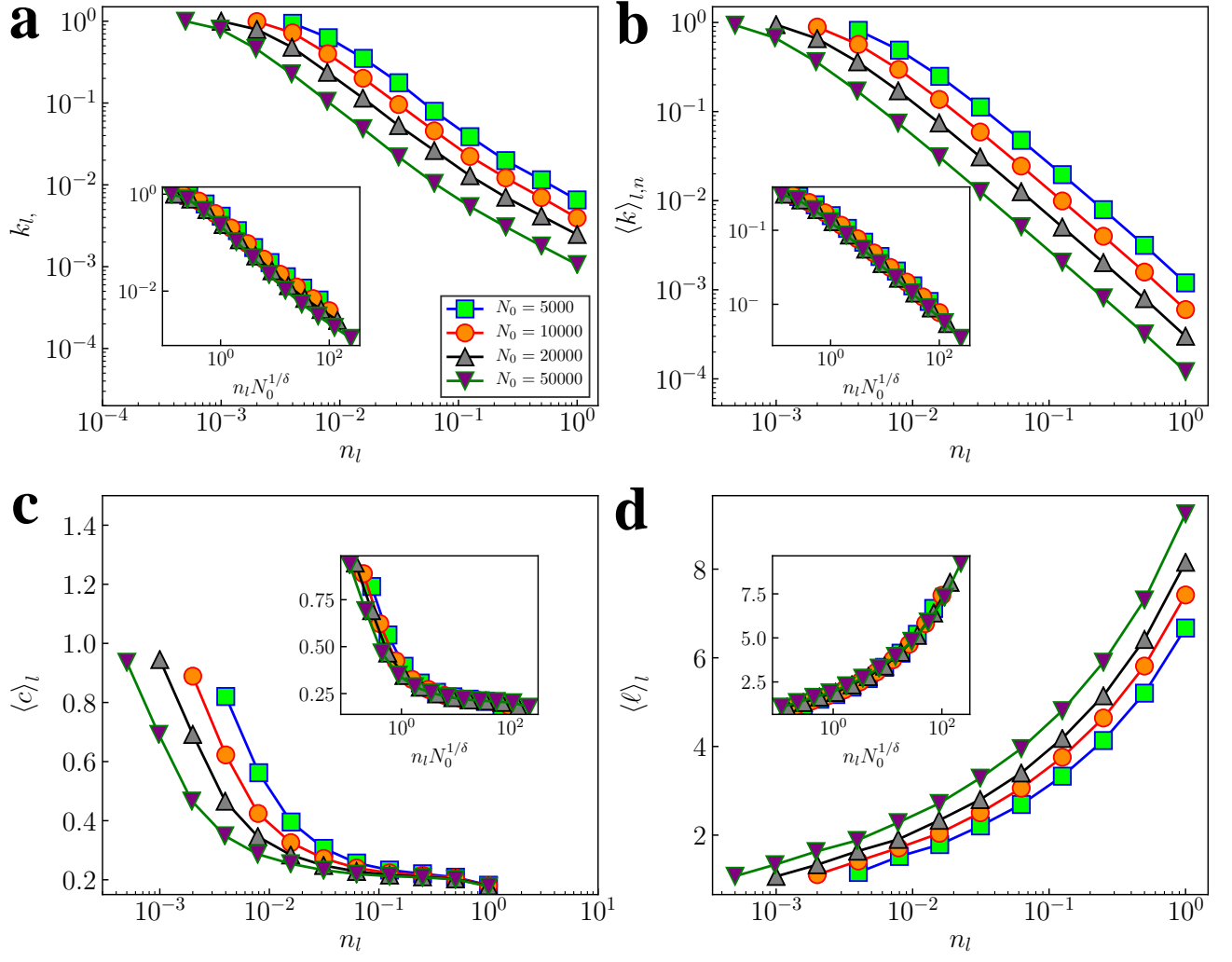


FIG. S8. FSS analysis of \mathbb{S}^D network topological observables along the GR flow, where $D = 2$. The main figures show each observable as a function of the variable n_l in the process of GR transformation, and the inset shows their scaling functions related to the variable $n_l N_0^{1/\delta}$. Key parameters of the \mathbb{S}^D network are $\nu = 2.5$ and $\sigma = 1.5$, respectively; the scaling exponent corresponding to four observables is $\delta = 2 \pm 0.1$. The average hidden degree $\langle \kappa \rangle_0 \approx 6$ and the expected average degree $\langle k \rangle_0 \approx 6$ for all initial networks. All the results are averaged over 10 independent realizations.

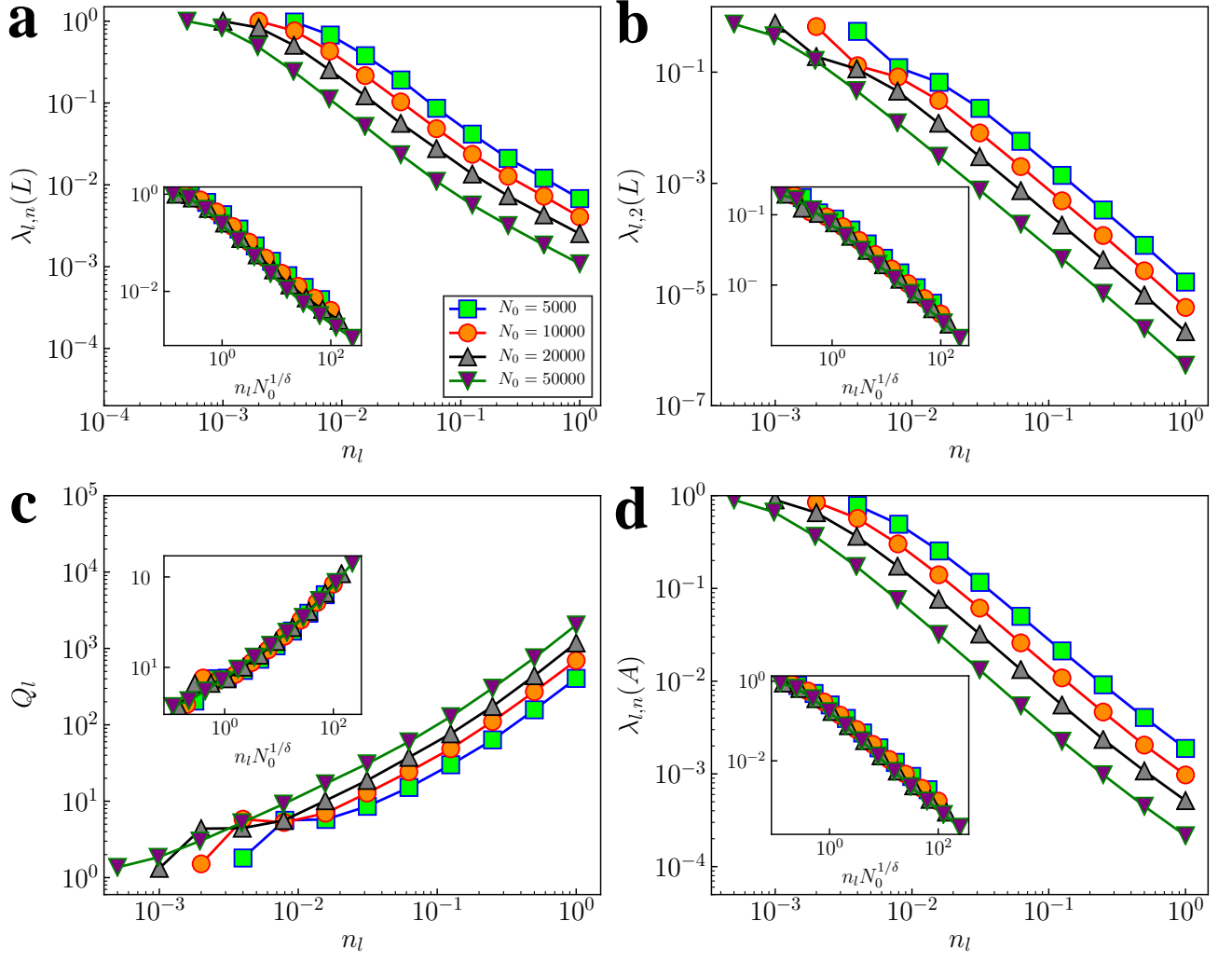


FIG. S9. FSS analysis of \mathbb{S}^D network dynamical observables along the GR flow, where $D = 2$. The main figures show each observable as a function of the variable n_l in the process of GR transformation, and the inset shows their scaling functions related to the variable $n_l N_0^{1/\delta}$. Key parameters of the \mathbb{S}^D network are $\nu = 2.5$ and $\sigma = 1.5$, respectively; the scaling exponent corresponding to four observables is $\delta = 2 \pm 0.1$. The average hidden degree $\langle \kappa \rangle_0 \approx 6$ and the expected average degree $\langle k \rangle_0 \approx 6$ for all initial networks. All the results are averaged over 10 independent realizations.

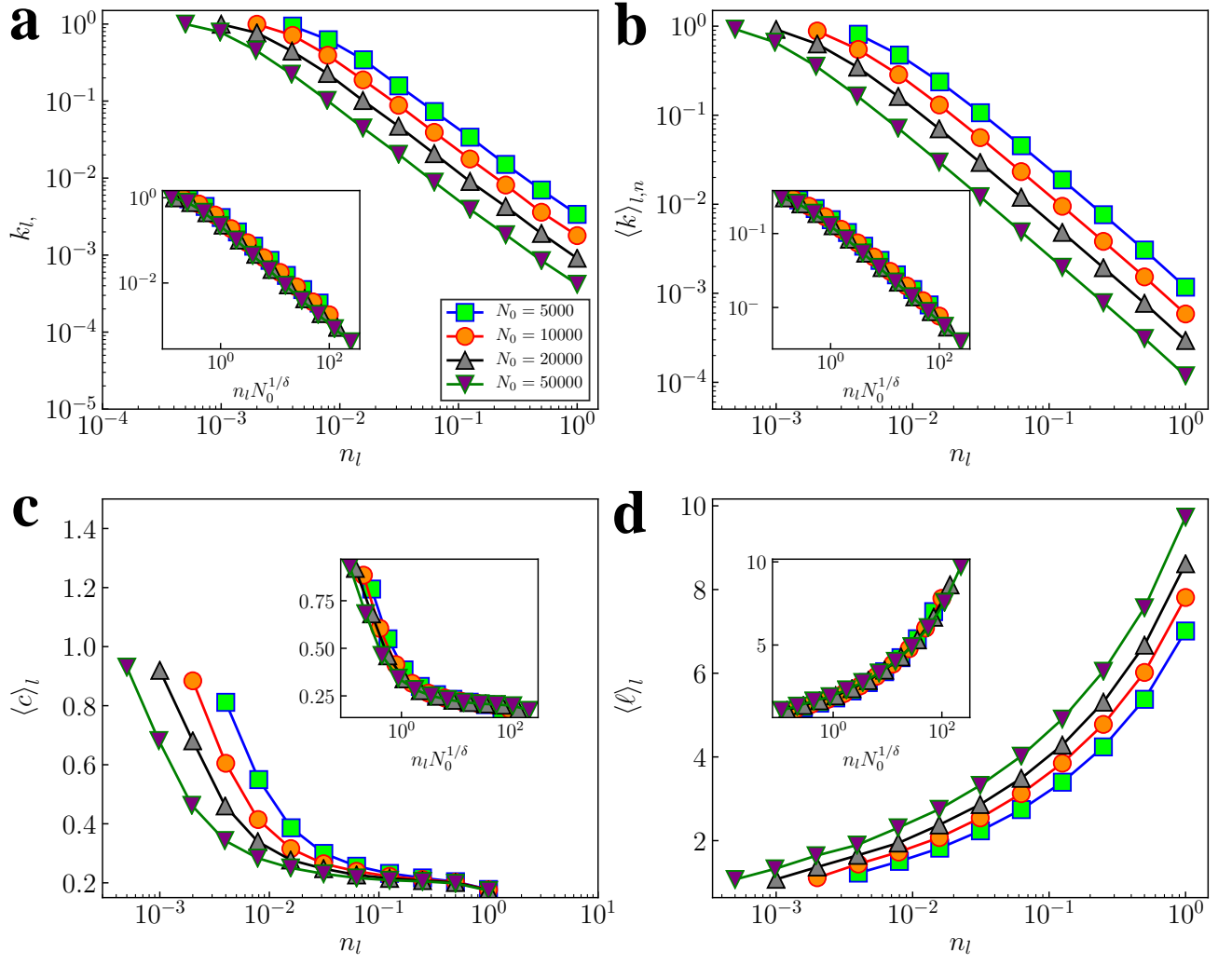


FIG. S10. FSS analysis of \mathbb{S}^D network topological observables along the GR flow, where $D = 5$. The main figures show each observable as a function of the variable n_l in the process of GR transformation, and the inset shows their scaling functions related to the variable $n_l N_0^{1/\delta}$. Key parameters of the \mathbb{S}^D network are $\nu = 2.5$ and $\sigma = 1.5$, respectively; the scaling exponent corresponding to four observables is $\delta = 2 \pm 0.1$. The average hidden degree $\langle \kappa \rangle_0 \approx 6$ and the expected average degree $\langle k \rangle_0 \approx 6$ for all initial networks. All the results are averaged over 10 independent realizations.

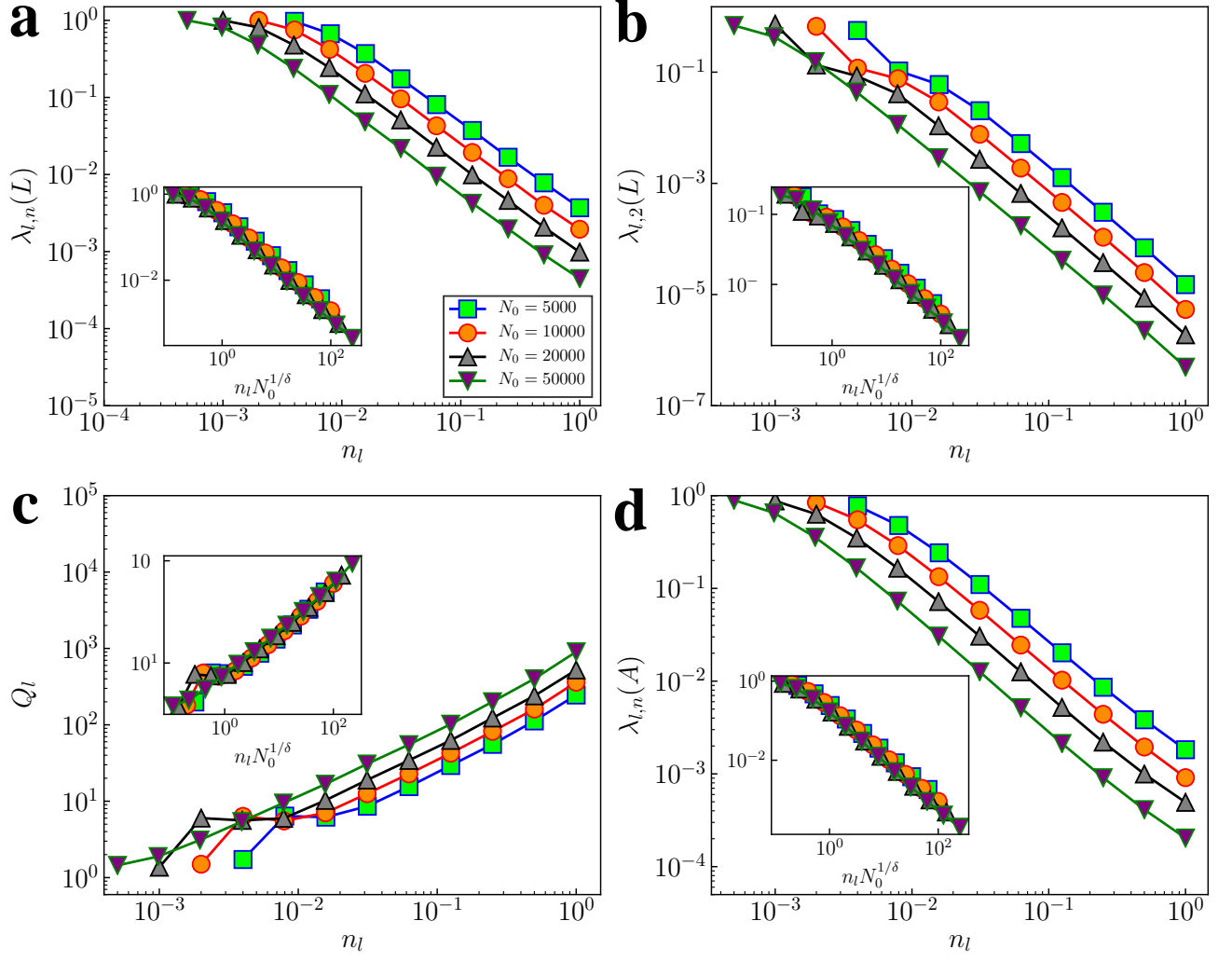


FIG. S11. FSS analysis of \mathbb{S}^D network dynamical observables along the GR flow, where $D = 5$. The main figures show each observable as a function of the variable n_l in the process of GR transformation, and the inset shows their scaling functions related to the variable $n_l N_0^{1/\delta}$. Key parameters of the \mathbb{S}^D network are $\nu = 2.5$ and $\sigma = 1.5$, respectively; the scaling exponent corresponding to four observables is $\delta = 2 \pm 0.1$. The average hidden degree $\langle \kappa \rangle_0 \approx 6$ and the expected average degree $\langle k \rangle_0 \approx 6$ for all initial networks. All the results are averaged over 10 independent realizations.

B. Real evolutionary networks

We consider ten types evolutionary networks (including 39 networks): IG5, TF, Rajat, Gnutella peer-to-peer network [6, 7], Cage, Maragal, Route Views AS graphs [8], CAIDA AS graphs (2004-2007) [8] and Condensed matter collaborations [9] and Socfb-UC [10]. Among them, IG5, TF, Rajat, Cage, and Maragal [10] are collections of some Miscellaneous networks, see [url](#). The Socfb-UC network dataset is in the category of Facebook networks. Here, we only consider the unweighted, undirected, and without self-loops versions of these networks. The basic topological characteristics of these networks are shown in Table S3, where the parameter ν is the approximate value obtained by fitting the tail of the degree distribution curve, and the parameter σ is a parameter necessary to embed the real network into the synthetic network, which is inferred by the method in [11]. The parameters ν and σ determine the position of each network in the (ν, σ) plane. Our results indicate that these networks are all in phase **I** or **III**, that is, they belong to small-world networks. The URL column provides an online link to download the datasets and clicking on the url automatically opens the corresponding website.

	Name	N	E	ν	σ	$\langle c \rangle$	Phase	URL
1	IG5-9	538	4570	1.93	1.0056	0.0222	I	url
2	IG5-11	1692	22110	1.98	1.0085	0.0003	I	url
3	IG5-13	4731	91209	1.99	1.0096	0.0112	I	url
4	IG5-15	11987	323509	1.88	1.0062	0.0097	I	url
5	IG5-17	30162	1034600	1.83	1.0066	0.0135	I	url
6	TF13	1302	11044	6.05	1.0077	0.0356	III	url
7	TF14	3160	29668	5.74	1.0070	0.0164	III	url
8	TF15	7742	79848	5.43	1.0067	0.0081	III	url
9	TF16	19321	215942	5.14	1.0075	0.0035	III	url
10	TF17	48630	585951	4.96	1.0053	0.0018	III	url
11	Rajat06	10922	18061	2.30	2.3593	0.4438	I	url
12	Rajat07	14842	24571	2.27	2.3834	0.4439	I	url
13	Rajat08	19362	32081	2.25	2.3829	0.4440	I	url
14	Rajat09	24482	40591	2.24	2.4735	0.4440	I	url
15	Rajat10	30202	50101	2.22	2.4876	0.4441	I	url
16	Gnutella, Aug. 04, 2002	10876	39994	3.39	1.0061	0.0080	III	url
17	Gnutella, Aug. 25, 2002	22663	54693	4.36	1.0070	0.0090	III	url
18	Gnutella, Aug. 30, 2002	36646	88303	5.65	1.0065	0.0114	III	url
19	Gnutella, Aug. 31, 2002	62561	147878	4.74	1.0077	0.0101	III	url
20	Cage9	3534	19030	6.16	1.5127	0.2095	III	url
21	Cage10	11397	69624	6.80	1.4405	0.1803	III	url
22	Cage11	39082	260320	6.46	1.4370	0.1736	III	url
23	Cage12	130228	951154	7.17	1.4232	0.1582	III	url
24	Maragal-2	549	4313	1.37	1.0058	0.1563	I	url
25	Maragal-3	1687	18246	1.35	1.0071	0.1787	I	url
26	Maragal-5	4654	92683	1.29	1.0055	0.1696	I	url
27	Maragal-6	21255	536283	1.23	1.0099	0.1208	I	url
28	AS-1998-01-02	3216	5705	2.35	1.0949	0.3311	I	url
29	AS-1999-12-06	6301	12226	2.50	1.2041	0.4006	I	url
30	AS-2001-05-26	11174	23409	2.55	1.3095	0.4532	I	url
31	CAIDA-2004-01-05	16301	32955	2.57	1.0474	0.3585	I	url
32	CAIDA-2006-01-30	21339	43283	2.58	1.1383	0.3648	I	url
33	CAIDA-2007-11-12	26389	52861	2.59	1.1289	0.3325	I	url
34	Cond-Mat, 1995-1999	13861	44619	2.82	5.5954	0.7194	I	url
35	Cond-Mat, 1995-2003	27519	116181	2.61	3.8944	0.7107	I	url
36	Cond-Mat, 1995-2005	36458	171735	2.51	3.6290	0.7079	I	url
37	Socfb-UC64	6810	155320	1.89	1.3660	0.2831	I	url
38	Socfb-UC61	13736	442169	1.94	1.3522	0.2714	I	url
39	Socfb-UC33	16800	522141	2.08	1.2898	0.2349	I	url

TABLE S3. Topology characteristics of real evolutionary networks. For each network, we report the network name, the number of nodes of the largest connected component, the number of edges of the largest connected component, the value of the exponent ν , the value of the parameter σ , the average clustering coefficient, the phase of the network, and the URL link of the network data that can be downloaded online.

Next, we investigate the complementary cumulative distribution function, the probability distribution function and the degree-dependent node clustering coefficient of each type of real evolutionary network, as well as the FSS analysis of each network under GR flow (see Figs. S12-S38). Our results show that a series of evolutionary networks of each type are approximately self-similar, and the scaling exponent of their eight observables is approximately equal to that of synthetic networks in the small-world phase, that is, $\delta \approx 2$.

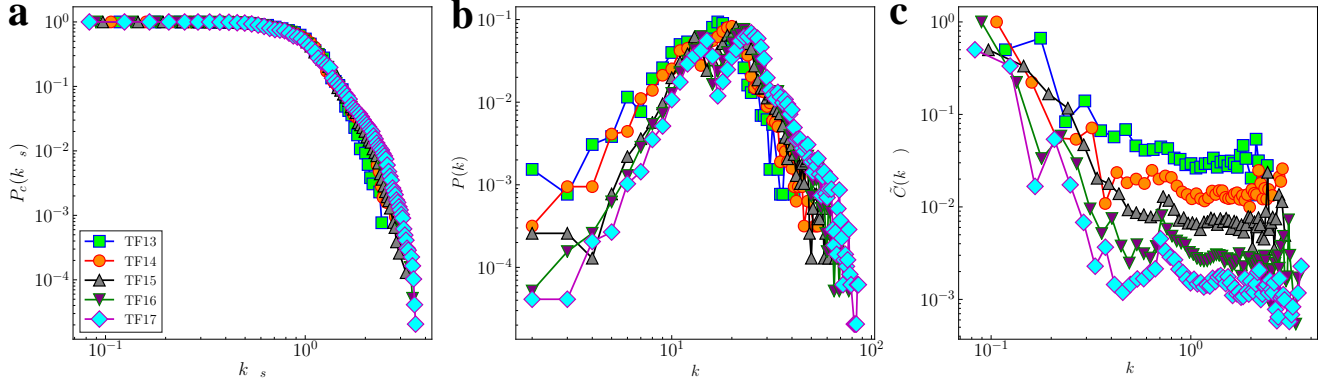


FIG. S12. Self-similarity of TF evolutionary networks. a The complementary cumulative distribution function (CCDF) P_c of node rescaled degrees $k_{res} = k/\langle k \rangle$. b The probability distribution function (PDF) $P(k)$ of the degree of nodes. c The degree-dependent clustering coefficient $\tilde{C}(k_{res})$ of node rescaled degrees k_{res} . Topological characteristics of this series of evolutionary networks are given in Table S3.

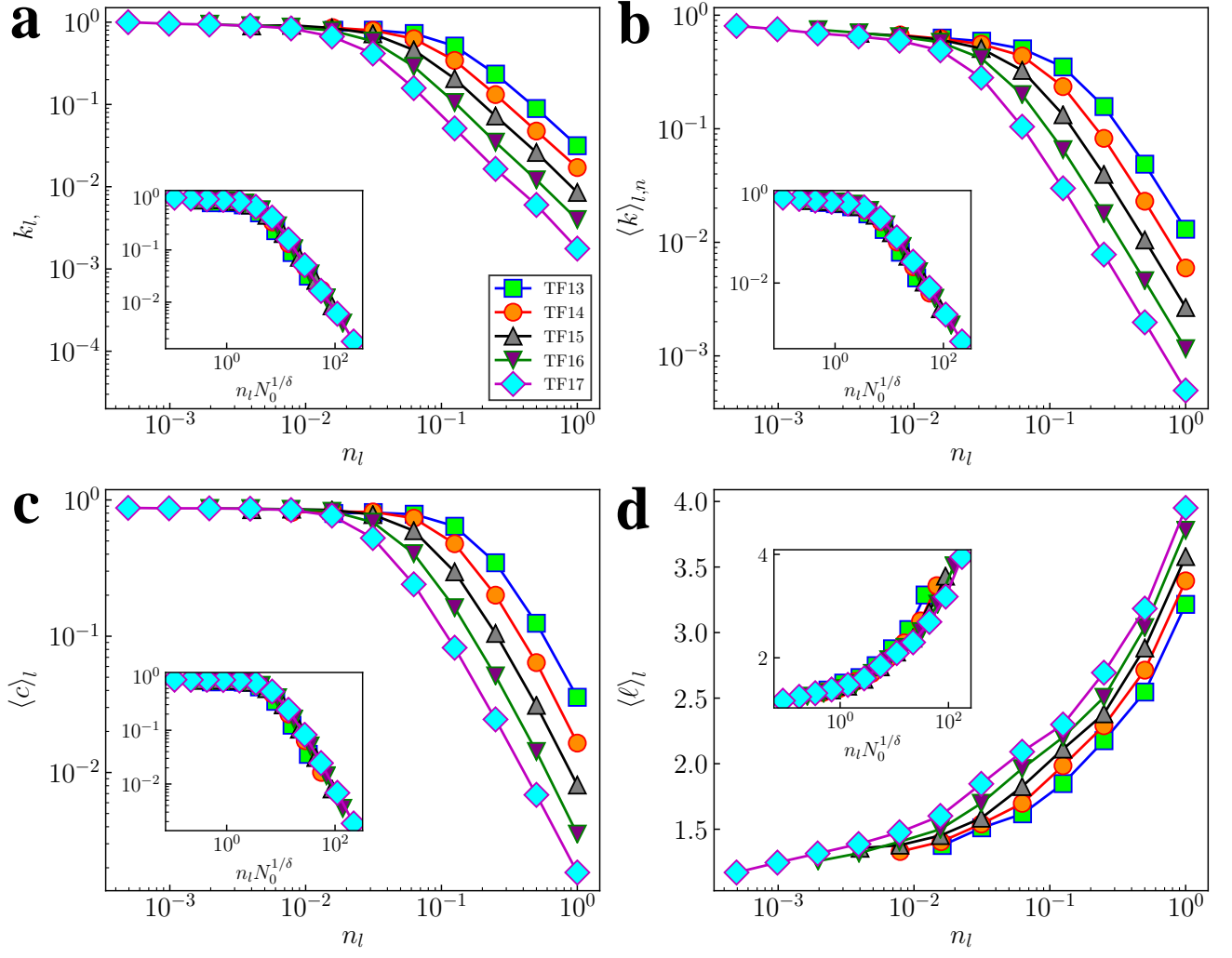


FIG. S13. FSS analysis of TF evolutionary networks' topological observables along the GR flow. The main figures show each observable as a function of the variable n_l in the process of GR transformation, and the inset shows their scaling functions related to the variable $n_l N_0^{1/\delta}$. These networks belong to phase **III**, and the scaling exponent corresponding to four observables is $\delta = 2 \pm 0.05$.

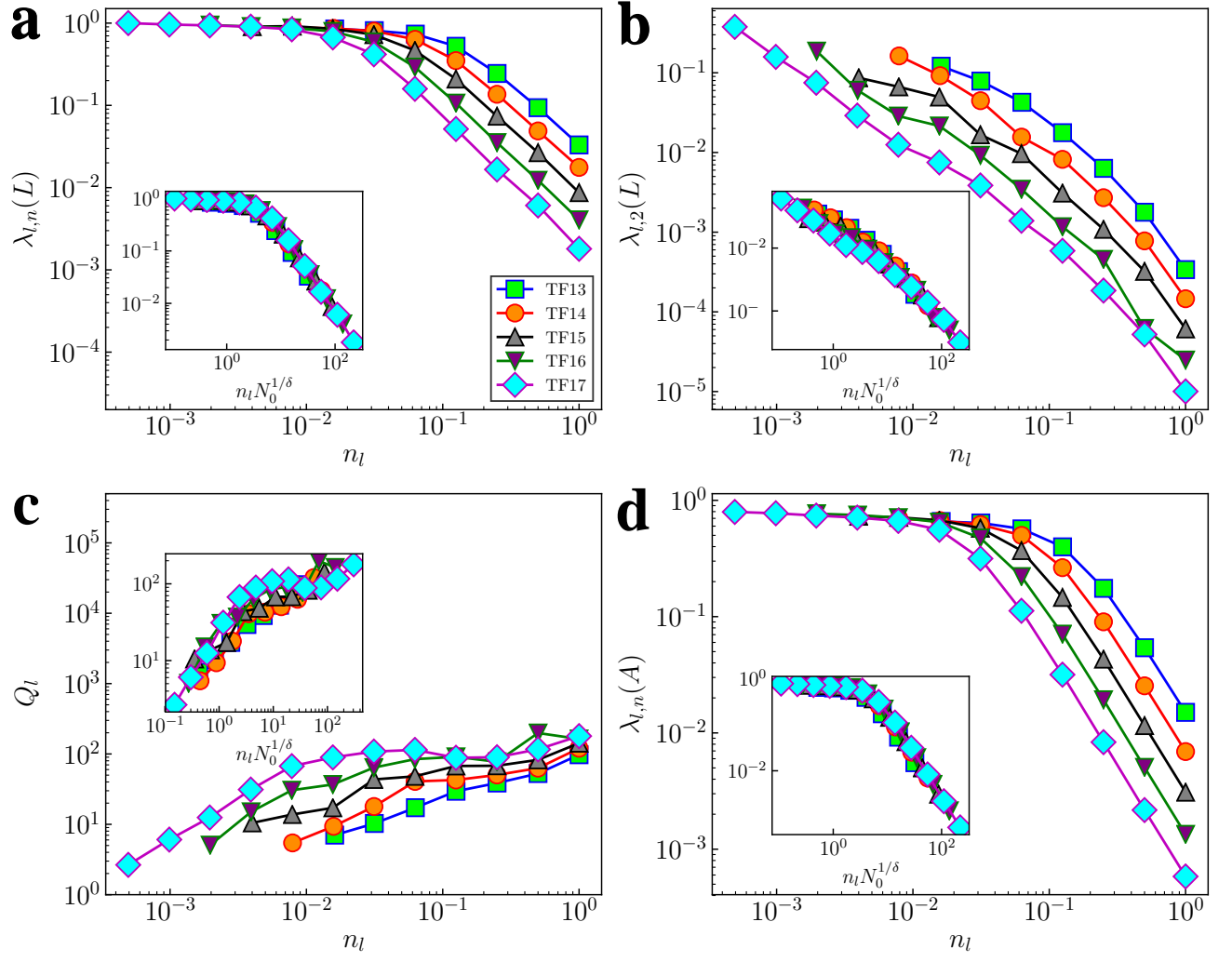


FIG. S14. FSS analysis of TF evolutionary networks' dynamical observables along the GR flow. The main figures show each observable as a function of the variable n_l in the process of GR transformation, and the inset shows their scaling functions related to the variable $n_l N_0^{1/\delta}$. The scaling exponent corresponding to four observables is $\delta = 2 \pm 0.1$.

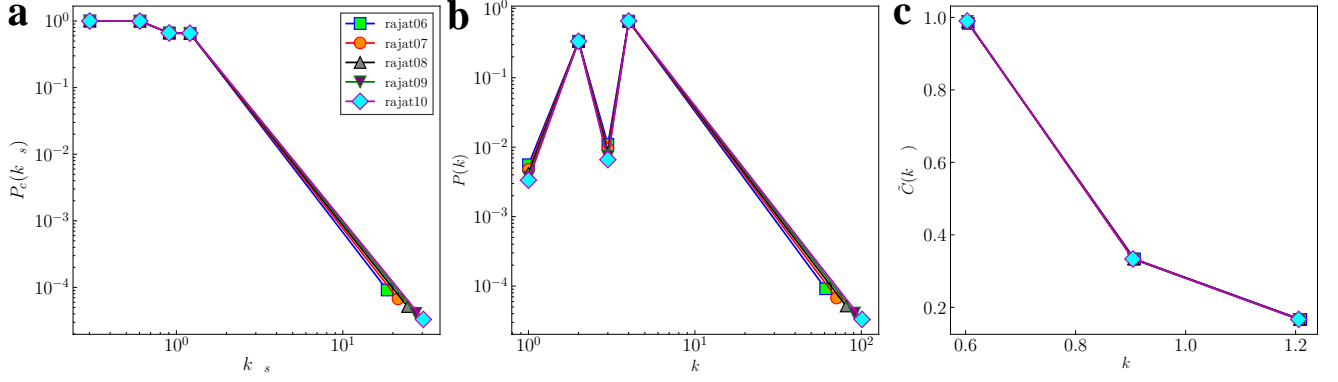


FIG. S15. Self-similarity of Rajat evolutionary networks. a The complementary cumulative distribution function (CCDF) P_c of node rescaled degrees $k_{res} = k/\langle k \rangle$. b The probability distribution function (PDF) $P(k)$ of the degree of nodes. c The degree-dependent clustering coefficient $\tilde{C}(k_{res})$ of node rescaled degrees k_{res} . Topological characteristics of this series of evolutionary networks are given in Table S3.

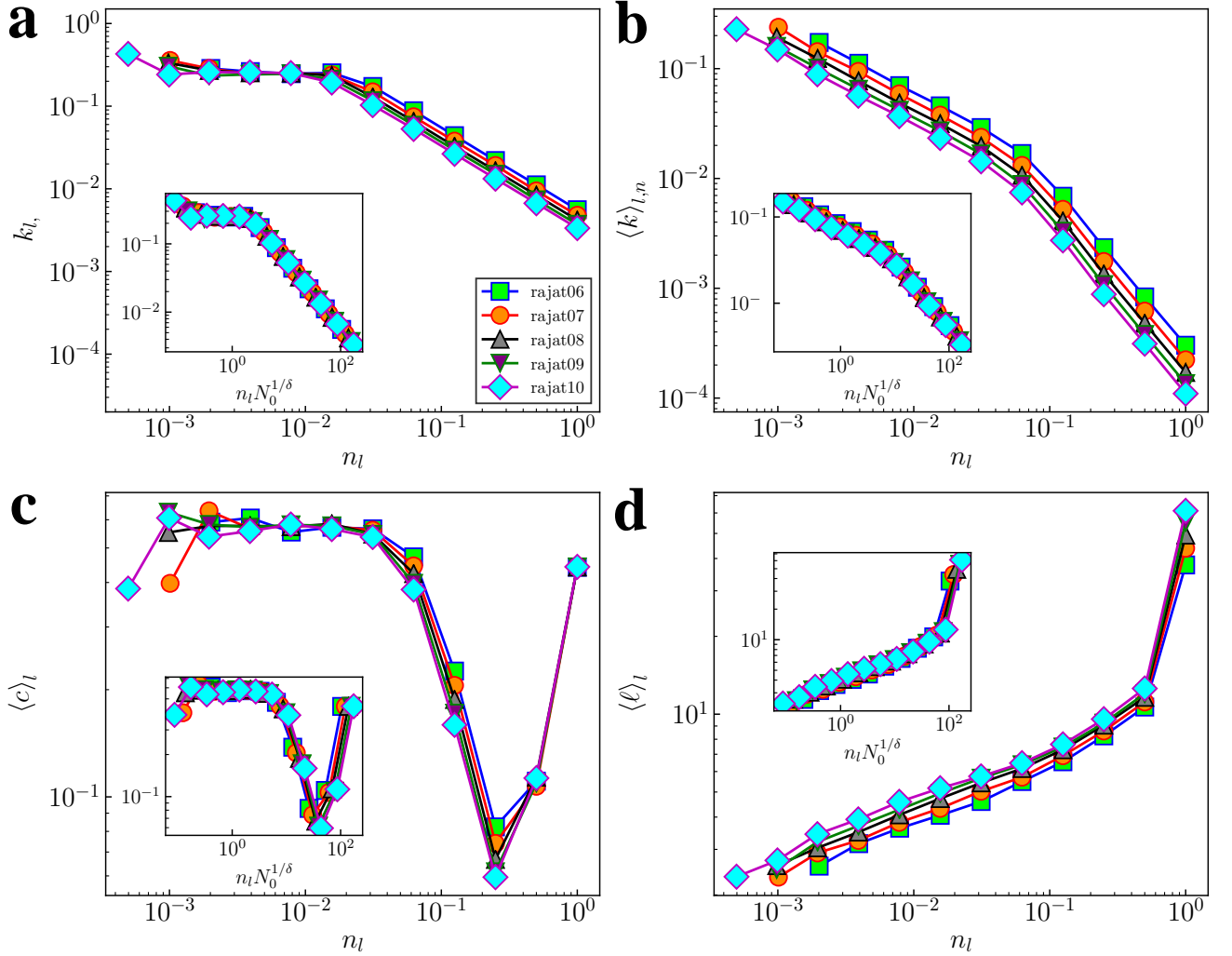


FIG. S16. FSS analysis of Rajat evolutionary networks' topological observables along the GR flow. The main figures show each observable as a function of the variable n_l in the process of GR transformation, and the inset shows their scaling functions related to the variable $n_l N_0^{1/\delta}$. These networks belong to phase I, and the scaling exponent corresponding to four observables is $\delta = 2$.

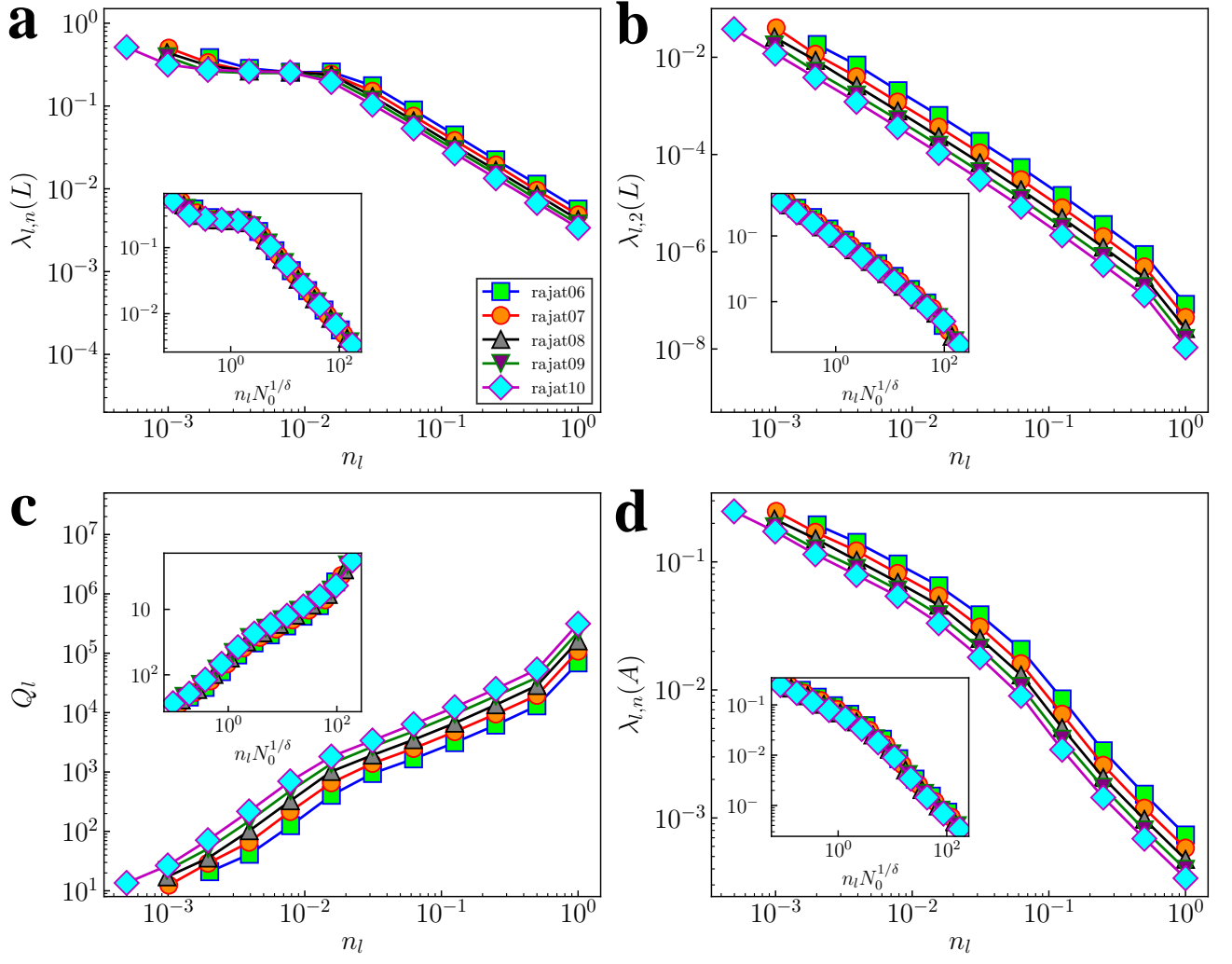


FIG. S17. FSS analysis of Rajat evolutionary networks' dynamical observables along the GR flow. The main figures show each observable as a function of the variable n_l in the process of GR transformation, and the inset shows their scaling functions related to the variable $n_l N_0^{1/\delta}$. The scaling exponent corresponding to four observables is $\delta = 2 \pm 0.05$.

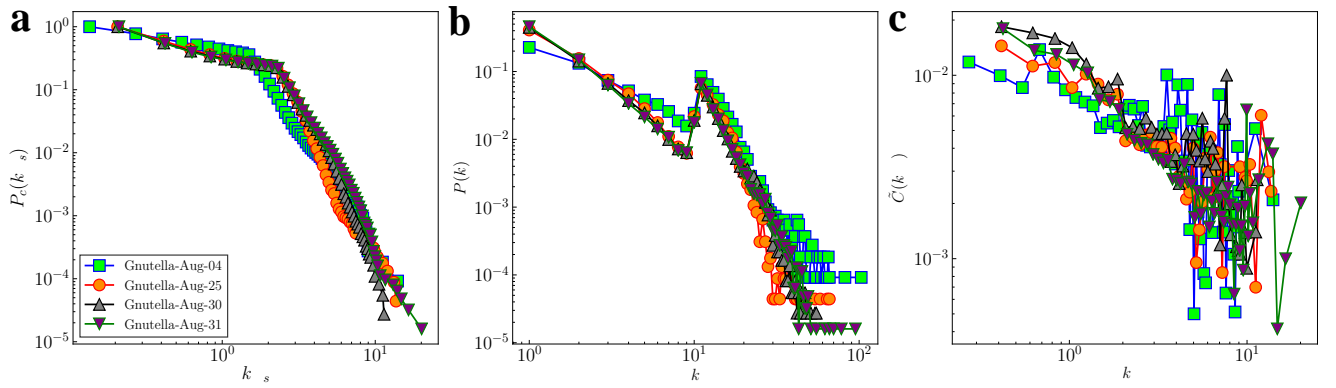


FIG. S18. Self-similarity of Gnutella peer-to-peer evolutionary networks. a The complementary cumulative distribution function (CCDF) P_c of node rescaled degrees $k_{res} = k/\langle k \rangle$. b The probability distribution function (PDF) $P(k)$ of the degree of nodes. c The degree-dependent clustering coefficient $\tilde{C}(k_{res})$ of node rescaled degrees k_{res} . Topological characteristics of this series of evolutionary networks are given in Table S3.

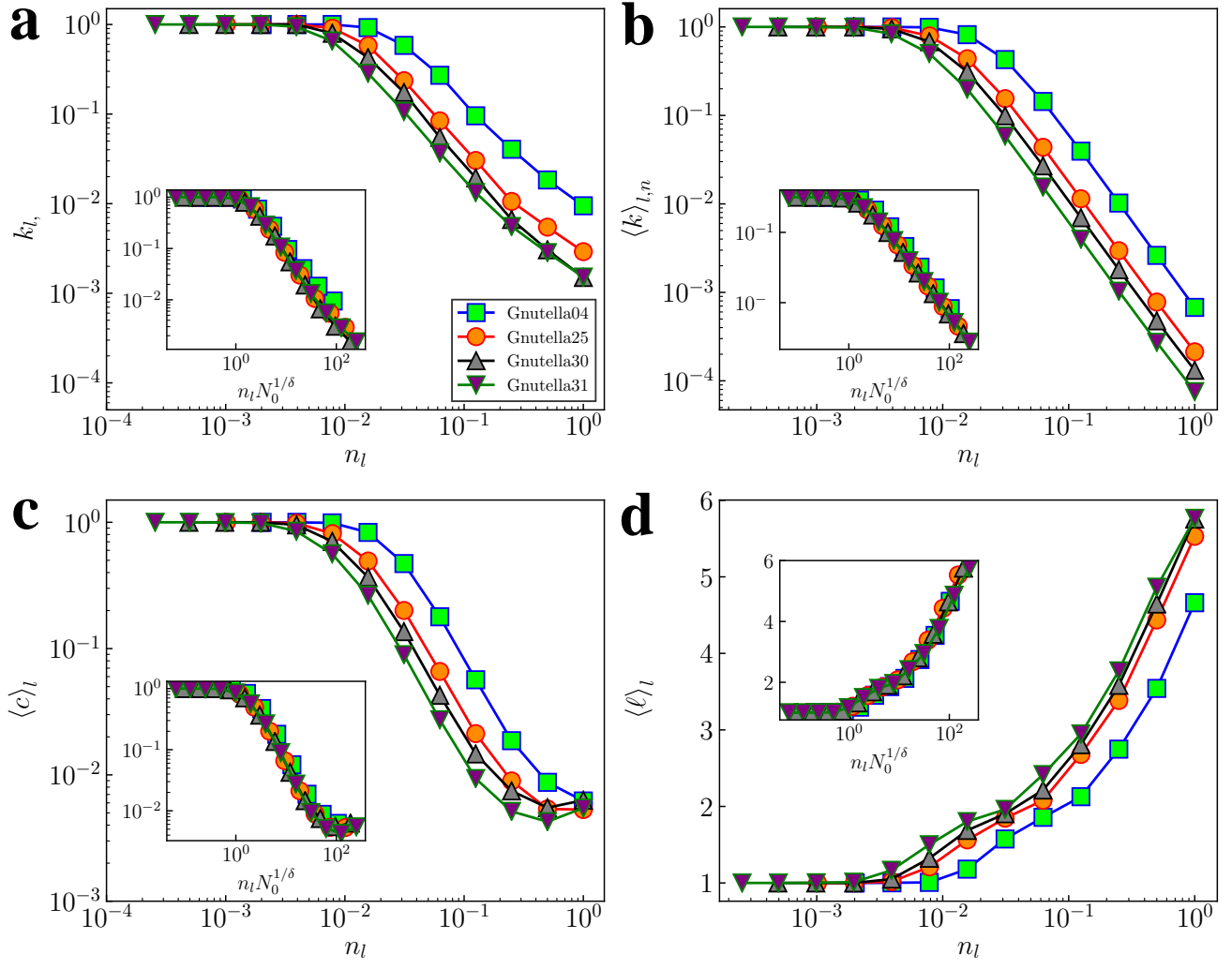


FIG. S19. FSS analysis of Gnutella peer-to-peer evolutionary networks' topological observables along the GR flow. The main figures show each observable as a function of the variable n_l in the process of GR transformation, and the inset shows their scaling functions related to the variable $n_l N_0^{1/\delta}$. These networks belong to phase **III**, and the scaling exponent corresponding to four observables is $\delta = 2 \pm 0.1$.

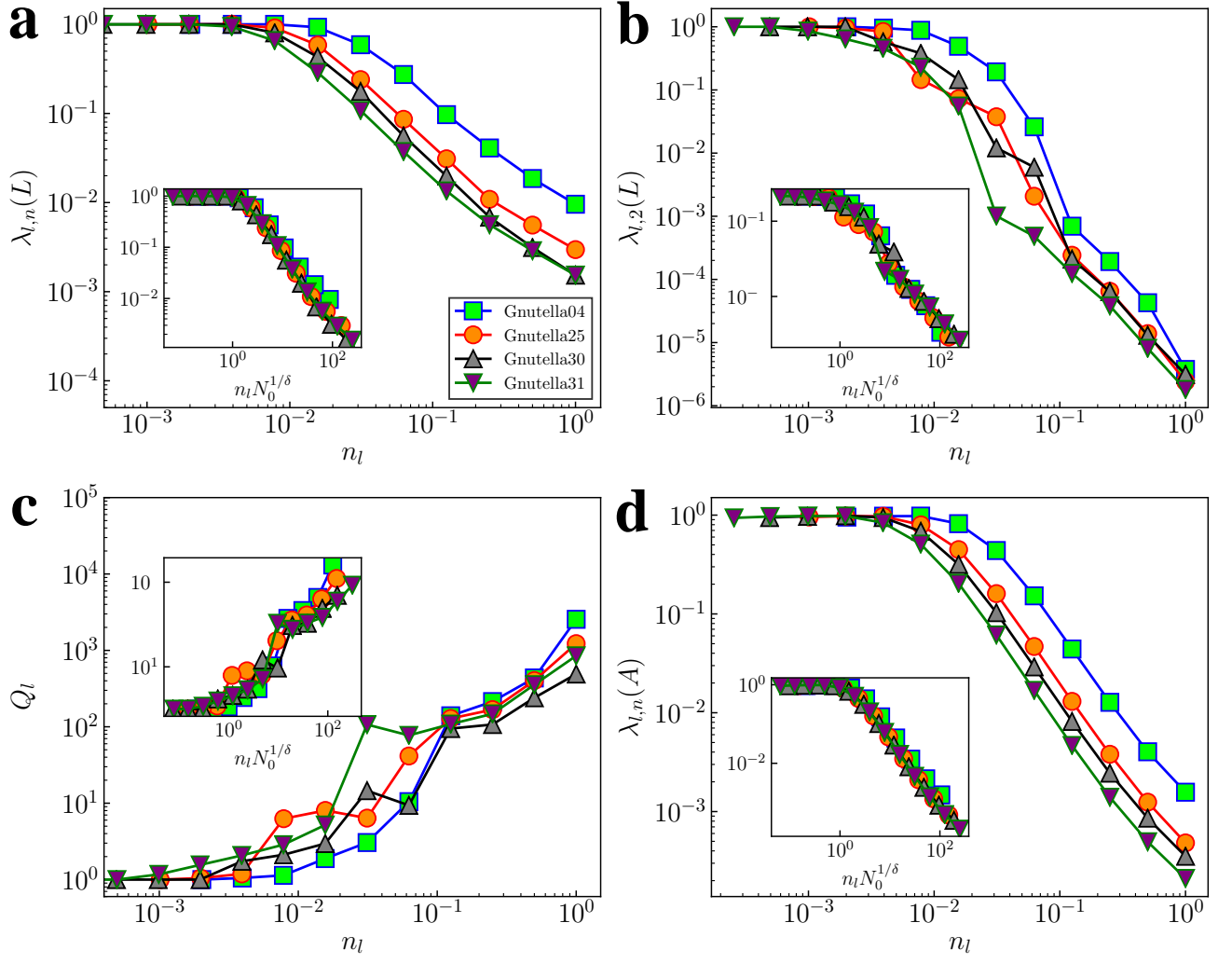


FIG. S20. FSS analysis of Gnutella peer-to-peer evolutionary networks' dynamical observables along the GR flow. The main figures show each observable as a function of the variable n_l in the process of GR transformation, and the inset shows their scaling functions related to the variable $n_l N_0^{1/\delta}$. The scaling exponent corresponding to four observables is $\delta = 2 \pm 0.1$.

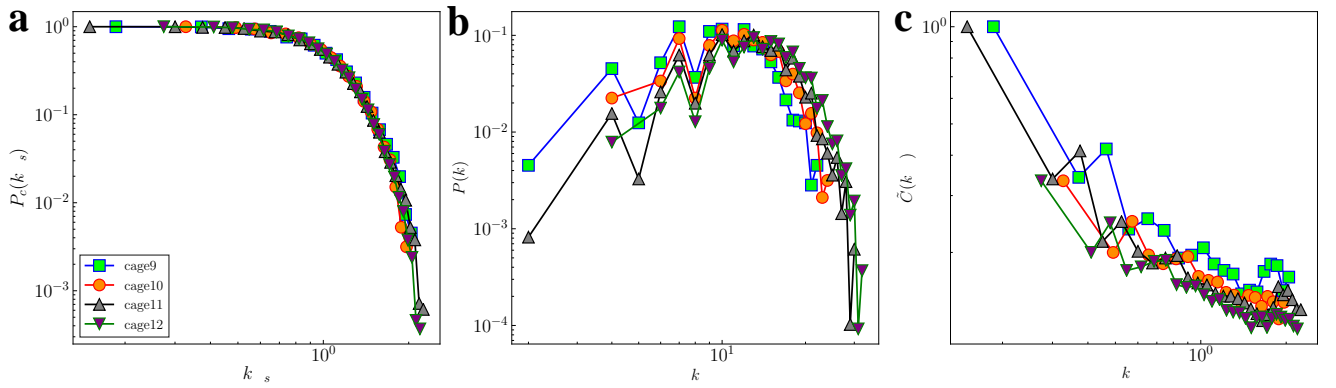


FIG. S21. Self-similarity of Cage evolutionary networks. a The complementary cumulative distribution function (CCDF) P_c of node rescaled degrees $k_{res} = k/\langle k \rangle$. b The probability distribution function (PDF) $P(k)$ of the degree of nodes. c The degree-dependent clustering coefficient $\tilde{C}(k_{res})$ of node rescaled degrees k_{res} . Topological characteristics of this series of evolutionary networks are given in Table S3.

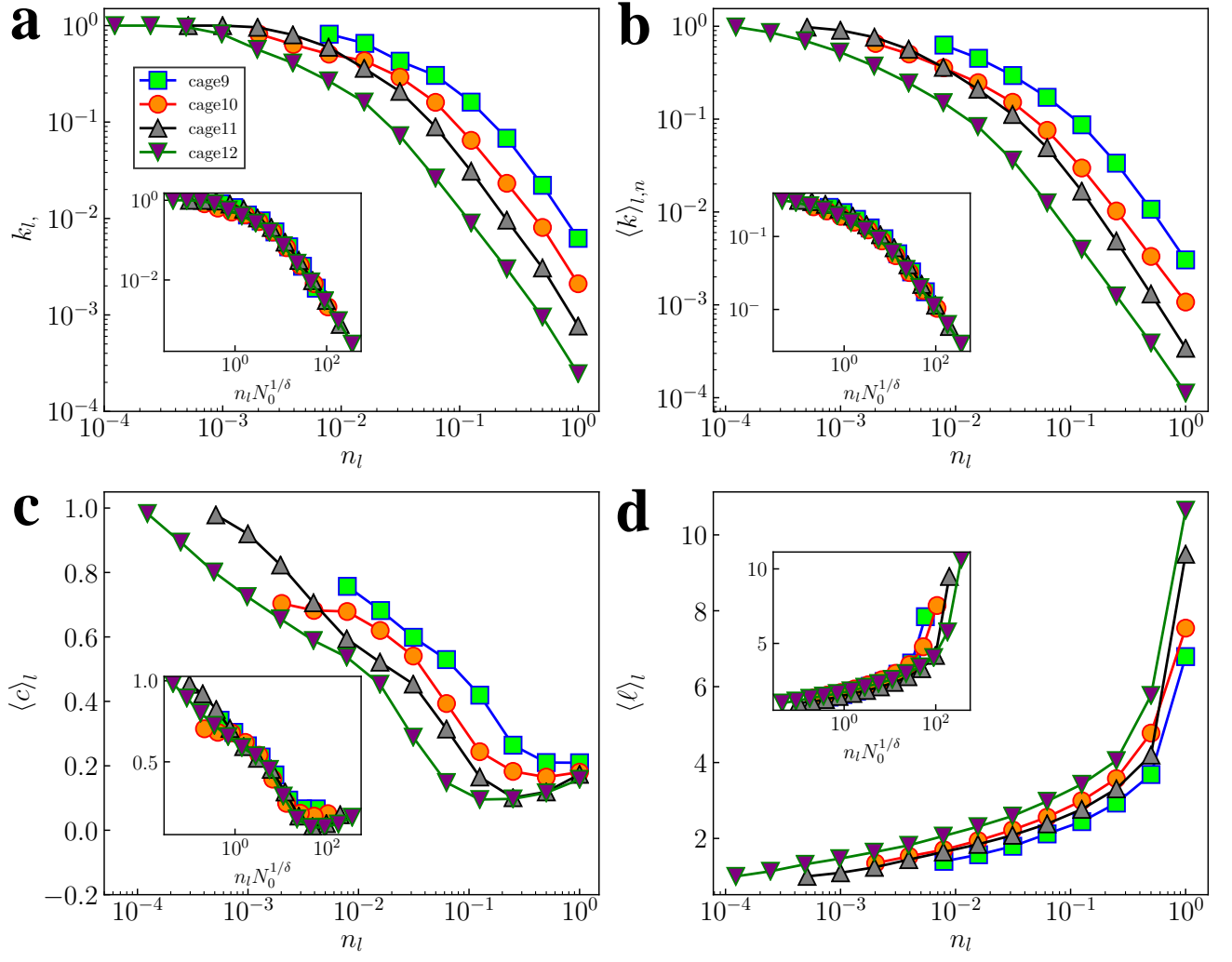


FIG. S22. FSS analysis of Cage evolutionary networks' topological observables along the GR flow. The main figures show each observable as a function of the variable n_l in the process of GR transformation, and the inset shows their scaling functions related to the variable $n_l N_0^{1/\delta}$. These networks belong to phase **III**, and the scaling exponent corresponding to four observables is $\delta = 2$.

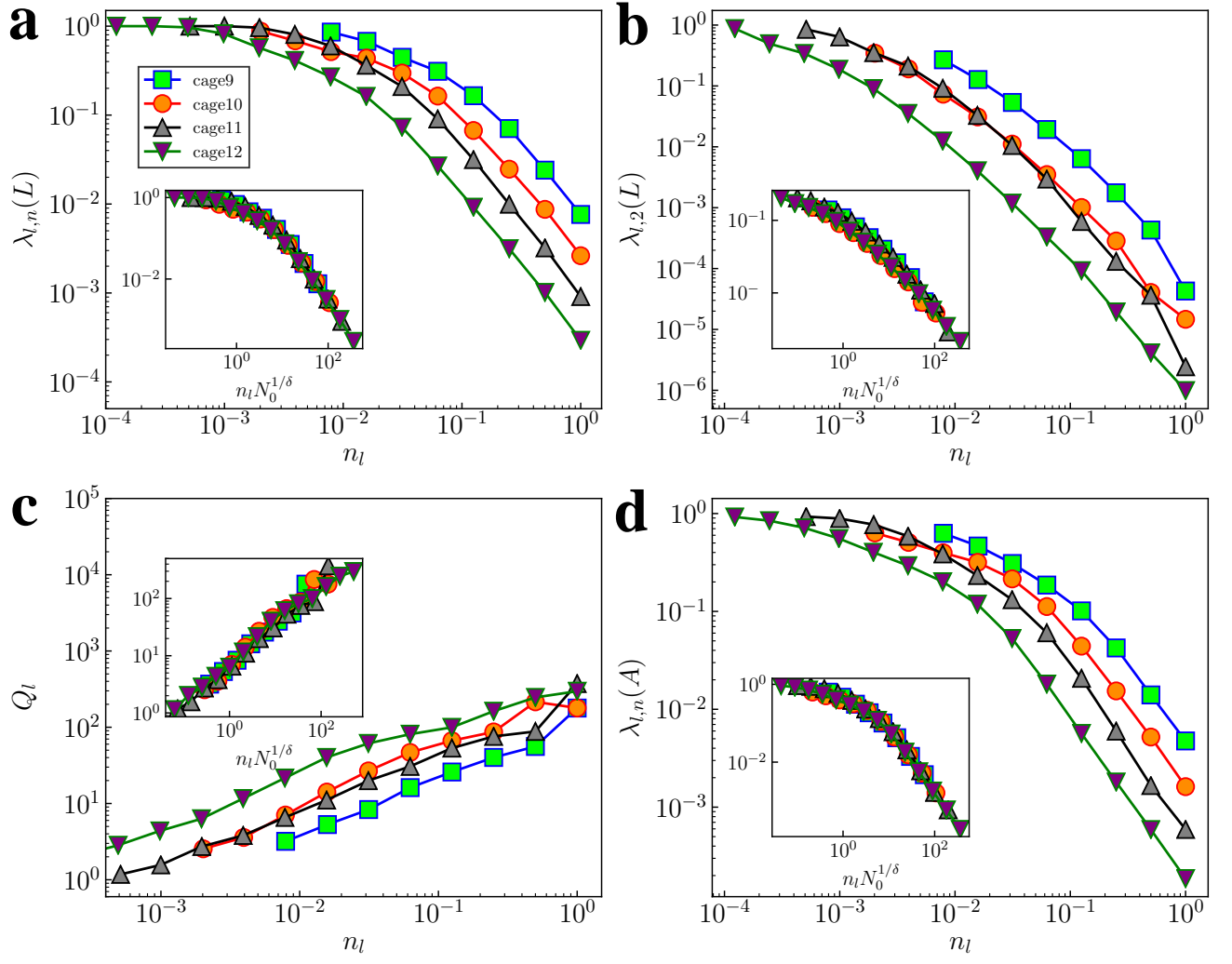


FIG. S23. FSS analysis of Cage evolutionary networks' dynamical observables along the GR flow. The main figures show each observable as a function of the variable n_l in the process of GR transformation, and the inset shows their scaling functions related to the variable $n_l N_0^{1/\delta}$. The scaling exponent corresponding to four observables is $\delta = 2 \pm 0.1$.

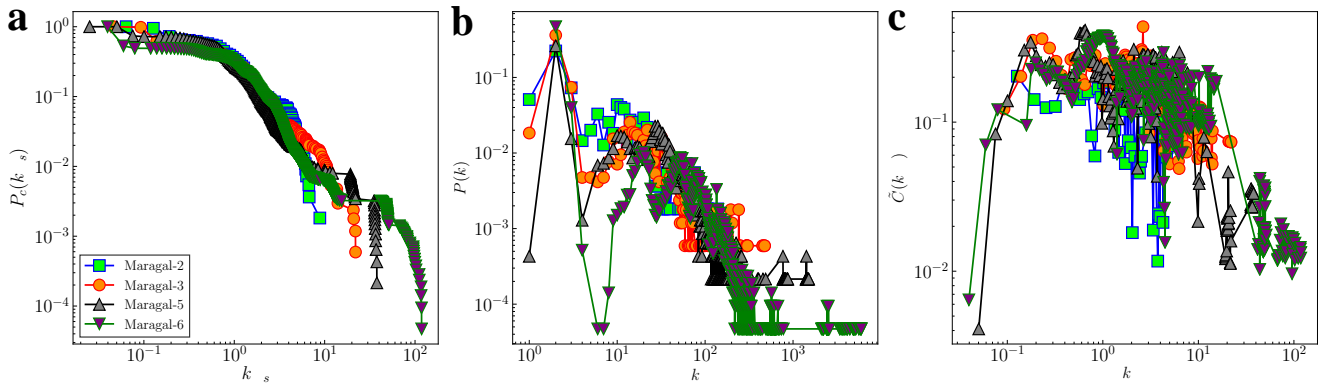


FIG. S24. Self-similarity of Maragal evolutionary networks. a The complementary cumulative distribution function (CCDF) P_c of node rescaled degrees $k_{res} = k/\langle k \rangle$. b The probability distribution function (PDF) $P(k)$ of the degree of nodes. c The degree-dependent clustering coefficient $\tilde{C}(k_{res})$ of node rescaled degrees k_{res} . Topological characteristics of this series of evolutionary networks are given in Table S3.

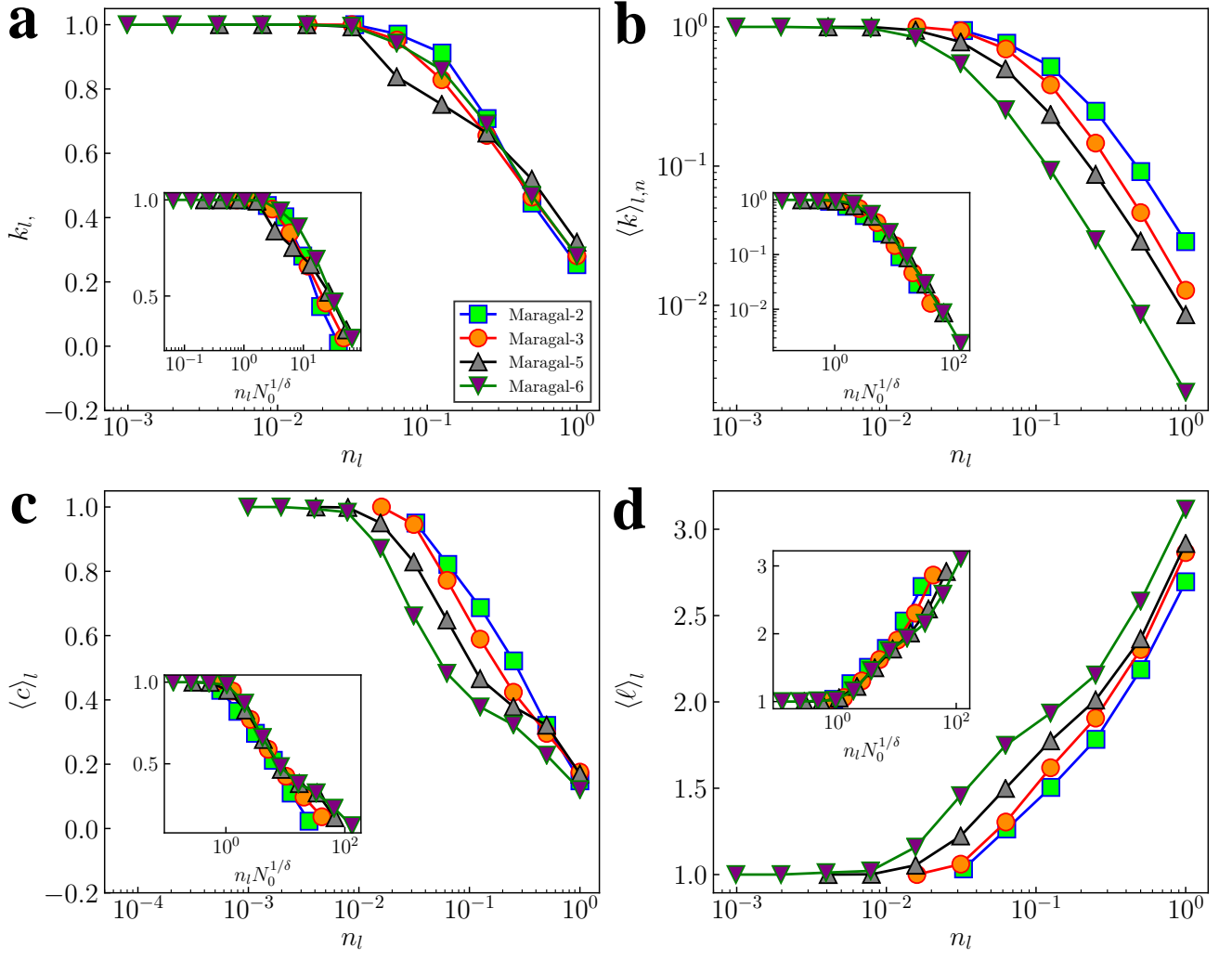


FIG. S25. FSS analysis of Maragal evolutionary networks' topological observables along the GR flow. The main figures show each observable as a function of the variable n_l in the process of GR transformation, and the inset shows their scaling functions related to the variable $n_l N_0^{1/\delta}$. These networks belong to phase I, and the scaling exponent corresponding to four observables is $\delta = 2 \pm 0.2$.

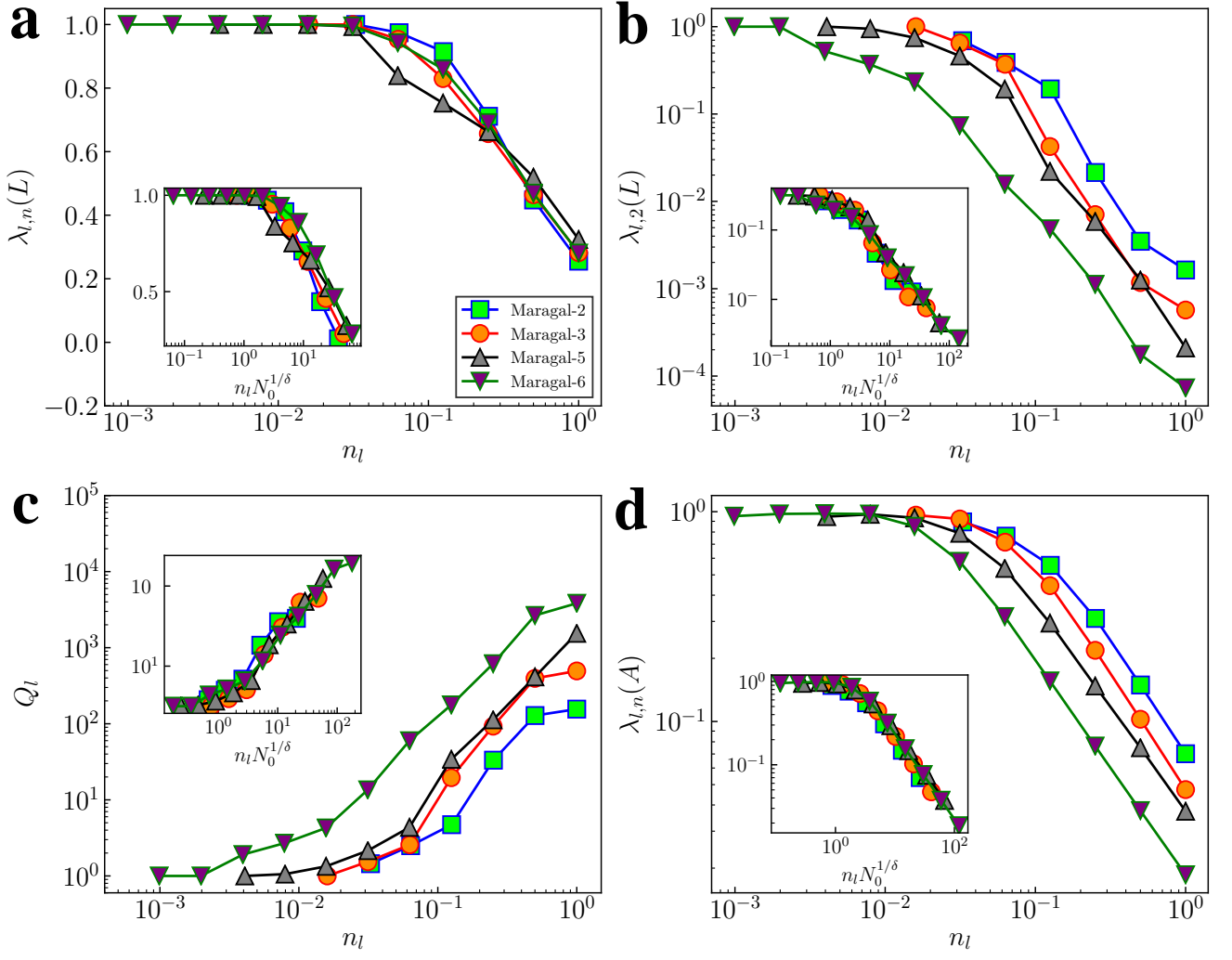


FIG. S26. FSS analysis of Maragal evolutionary networks' dynamical observables along the GR flow. The main figures show each observable as a function of the variable n_l in the process of GR transformation, and the inset shows their scaling functions related to the variable $n_l N_0^{1/\delta}$. The scaling exponent corresponding to four observables is $\delta = 2 \pm 0.2$.

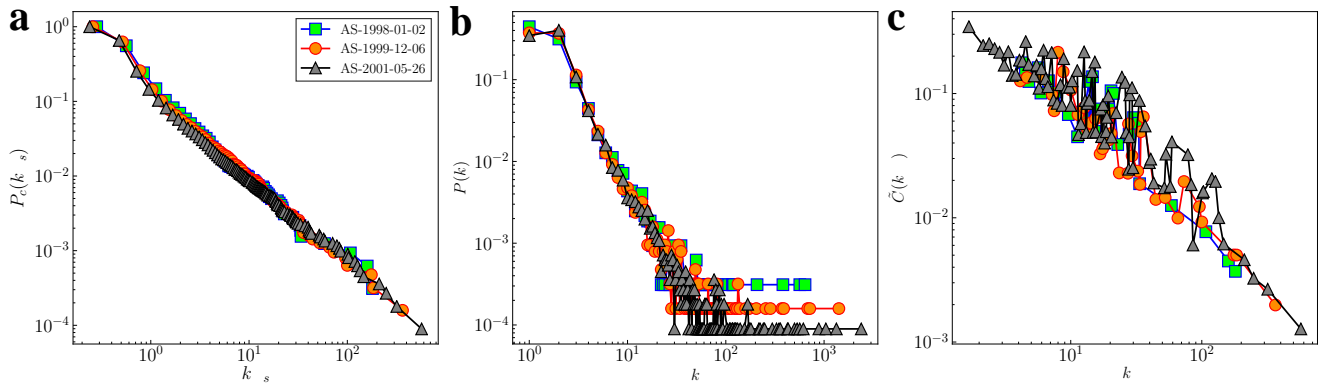


FIG. S27. Self-similarity of Route Views AS evolutionary networks. a The complementary cumulative distribution function (CCDF) P_c of node rescaled degrees $k_{res} = k/\langle k \rangle$. b The probability distribution function (PDF) $P(k)$ of the degree of nodes. c The degree-dependent clustering coefficient $\tilde{C}(k_{res})$ of node rescaled degrees k_{res} . Topological characteristics of this series of evolutionary networks are given in Table S3.

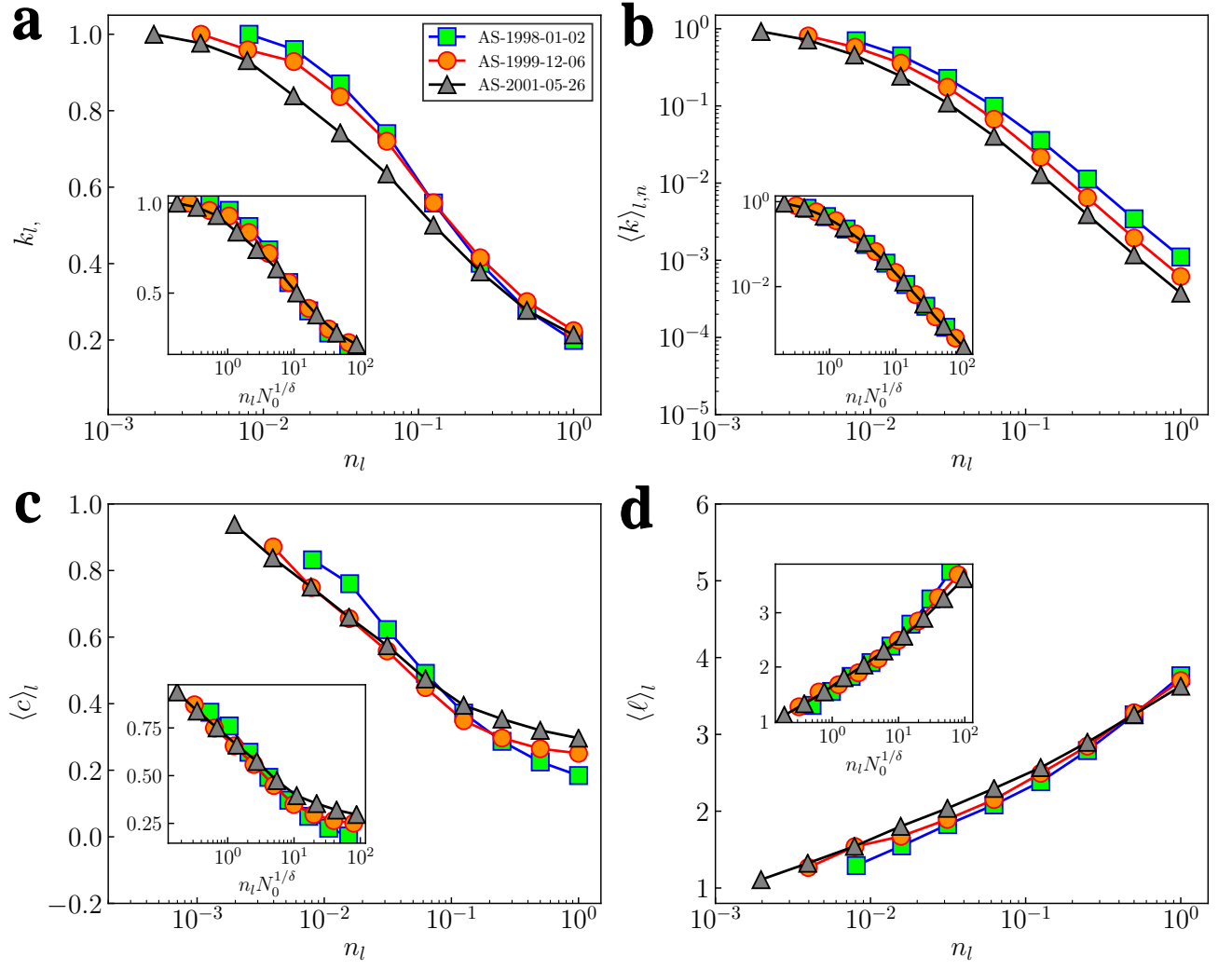


FIG. S28. FSS analysis of Route Views AS evolutionary networks' topological observables along the GR flow. The main figures show each observable as a function of the variable n_l in the process of GR transformation, and the inset shows their scaling functions related to the variable $n_l N_0^{1/\delta}$. These networks belong to phase **I**, and the scaling exponent corresponding to four observables is $\delta = 2 \pm 0.1$.

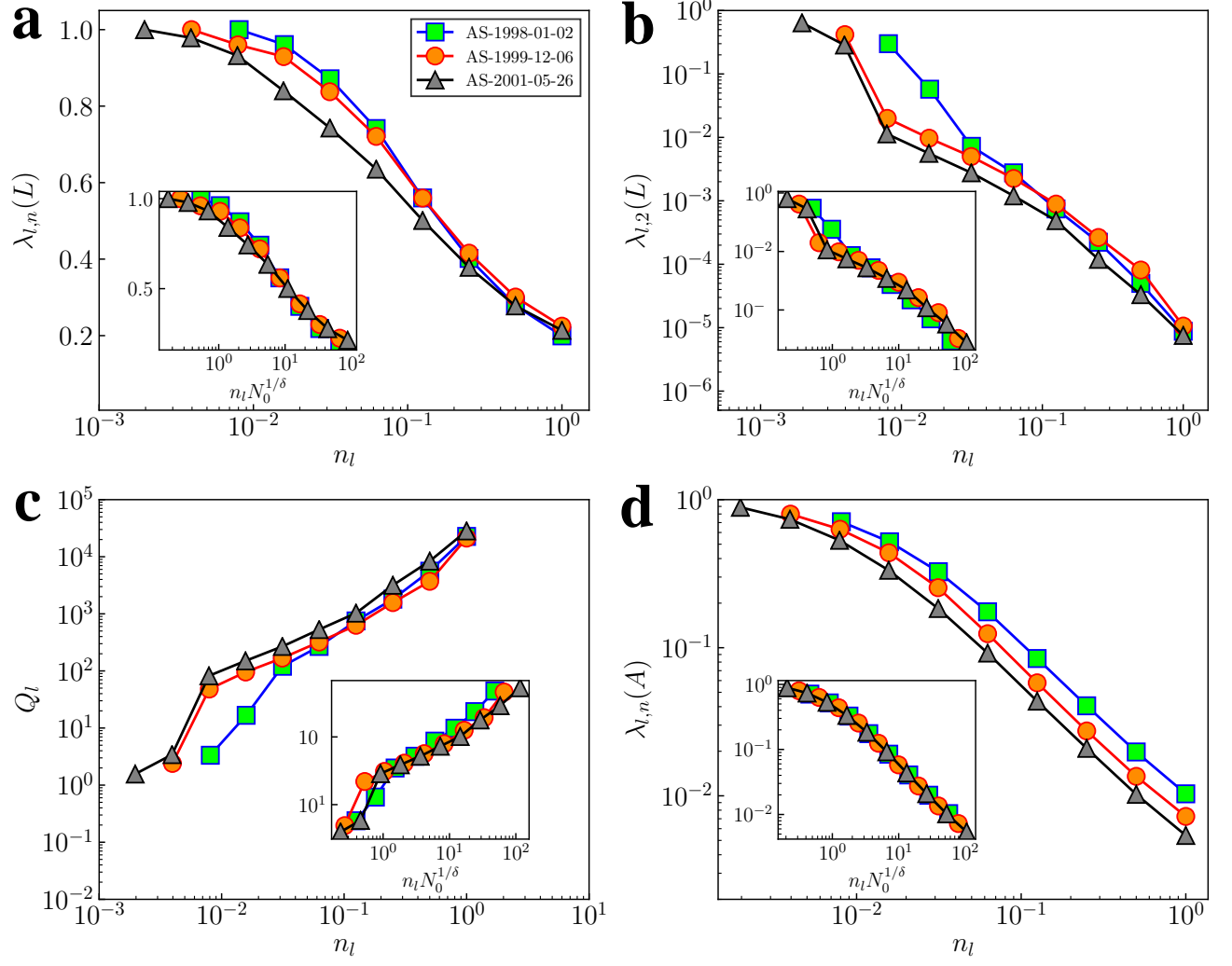


FIG. S29. FSS analysis of Route Views AS evolutionary networks' dynamical observables along the GR flow. The main figures show each observable as a function of the variable n_l in the process of GR transformation, and the inset shows their scaling functions related to the variable $n_l N_0^{1/\delta}$. The scaling exponent corresponding to four observables is $\delta = 2 \pm 0.1$.

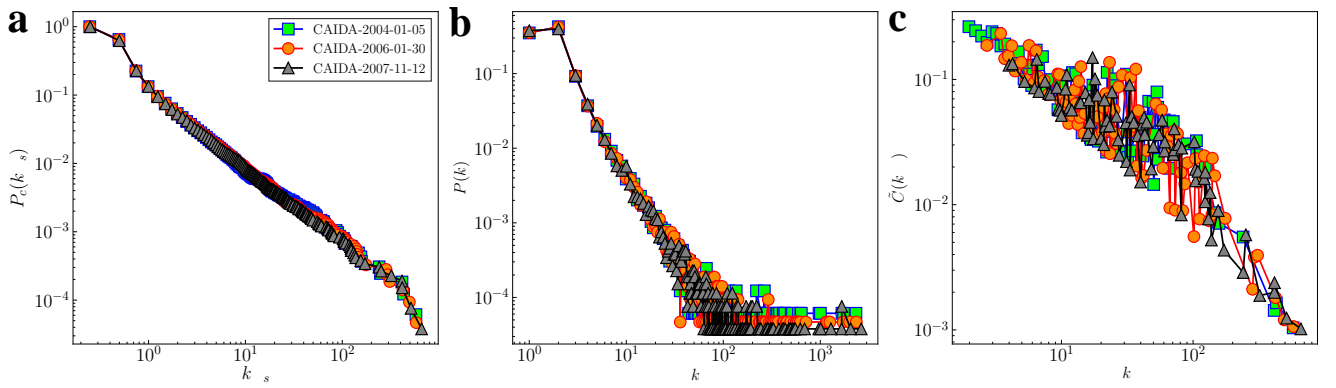


FIG. S30. Self-similarity of CAIDA AS evolutionary networks. a The complementary cumulative distribution function (CCDF) P_c of node rescaled degrees $k_{res} = k/\langle k \rangle$. b The probability distribution function (PDF) $P(k)$ of the degree of nodes. c The degree-dependent clustering coefficient $\tilde{C}(k_{res})$ of node rescaled degrees k_{res} . Topological characteristics of this series of evolutionary networks are given in Table S3.

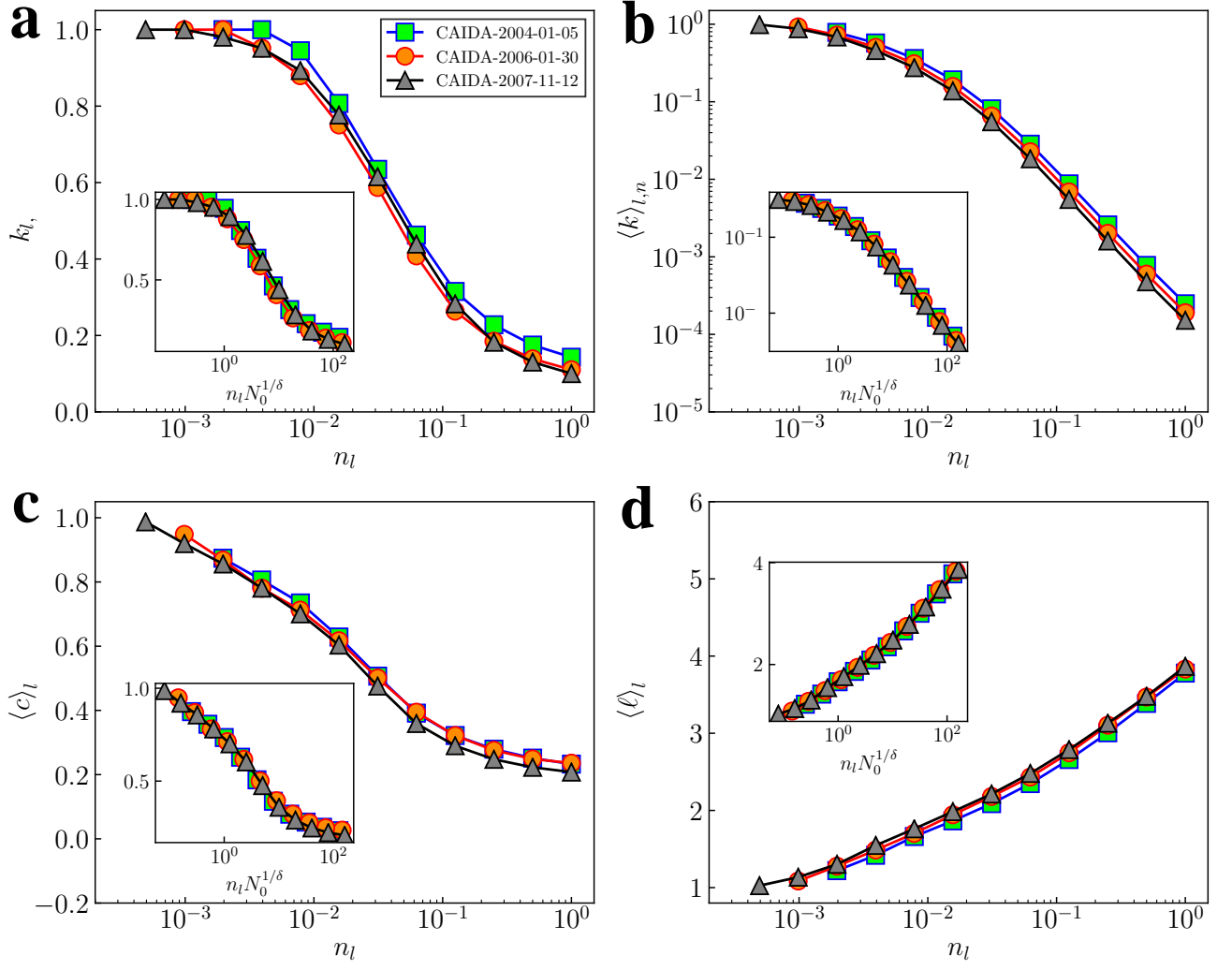


FIG. S31. FSS analysis of CAIDA AS evolutionary networks' topological observables along the GR flow. The main figures show each observable as a function of the variable n_l in the process of GR transformation, and the inset shows their scaling functions related to the variable $n_l N_0^{1/\delta}$. These networks belong to phase **I**, and the scaling exponent corresponding to four observables is $\delta = 2$.

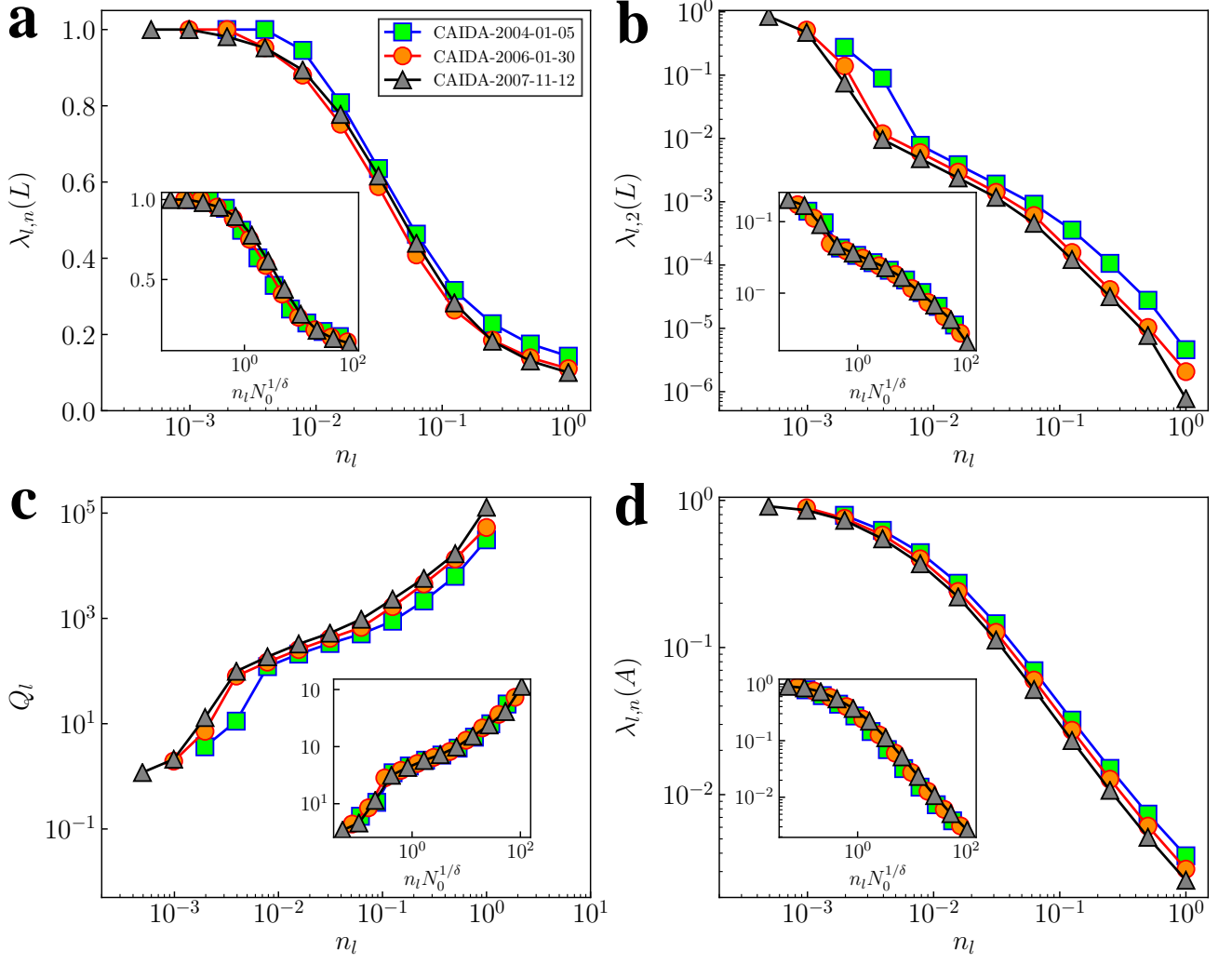


FIG. S32. FSS analysis of CAIDA AS evolutionary networks' dynamical observables along the GR flow. The main figures show each observable as a function of the variable n_l in the process of GR transformation, and the inset shows their scaling functions related to the variable $n_l N_0^{1/\delta}$. The scaling exponent corresponding to four observables is $\delta = 2 \pm 0.05$.

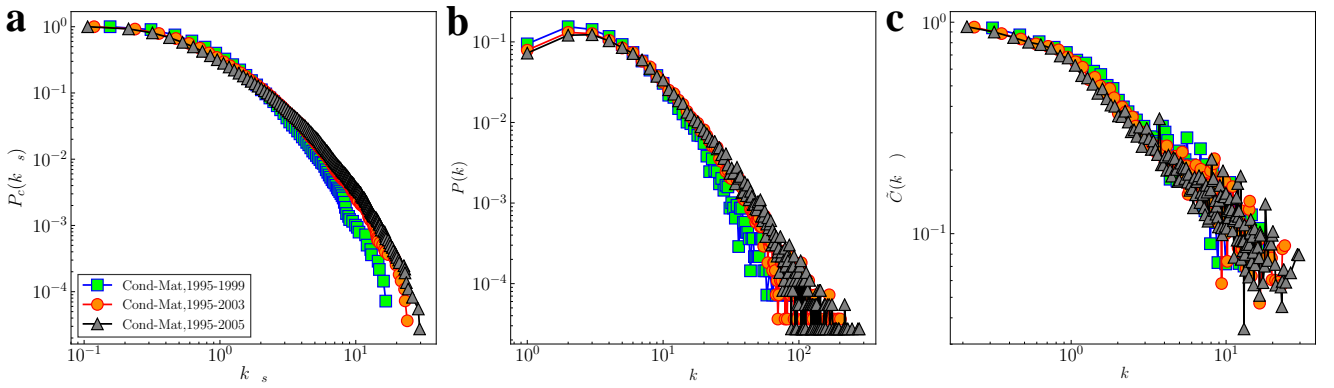


FIG. S33. Self-similarity of Condensed matter collaborations evolutionary networks. a The complementary cumulative distribution function (CCDF) P_c of node rescaled degrees $k_{res} = k/\langle k \rangle$. b The probability distribution function (PDF) $P(k)$ of the degree of nodes. c The degree-dependent clustering coefficient $\tilde{C}(k_{res})$ of node rescaled degrees k_{res} . Topological characteristics of this series of evolutionary networks are given in Table S3.

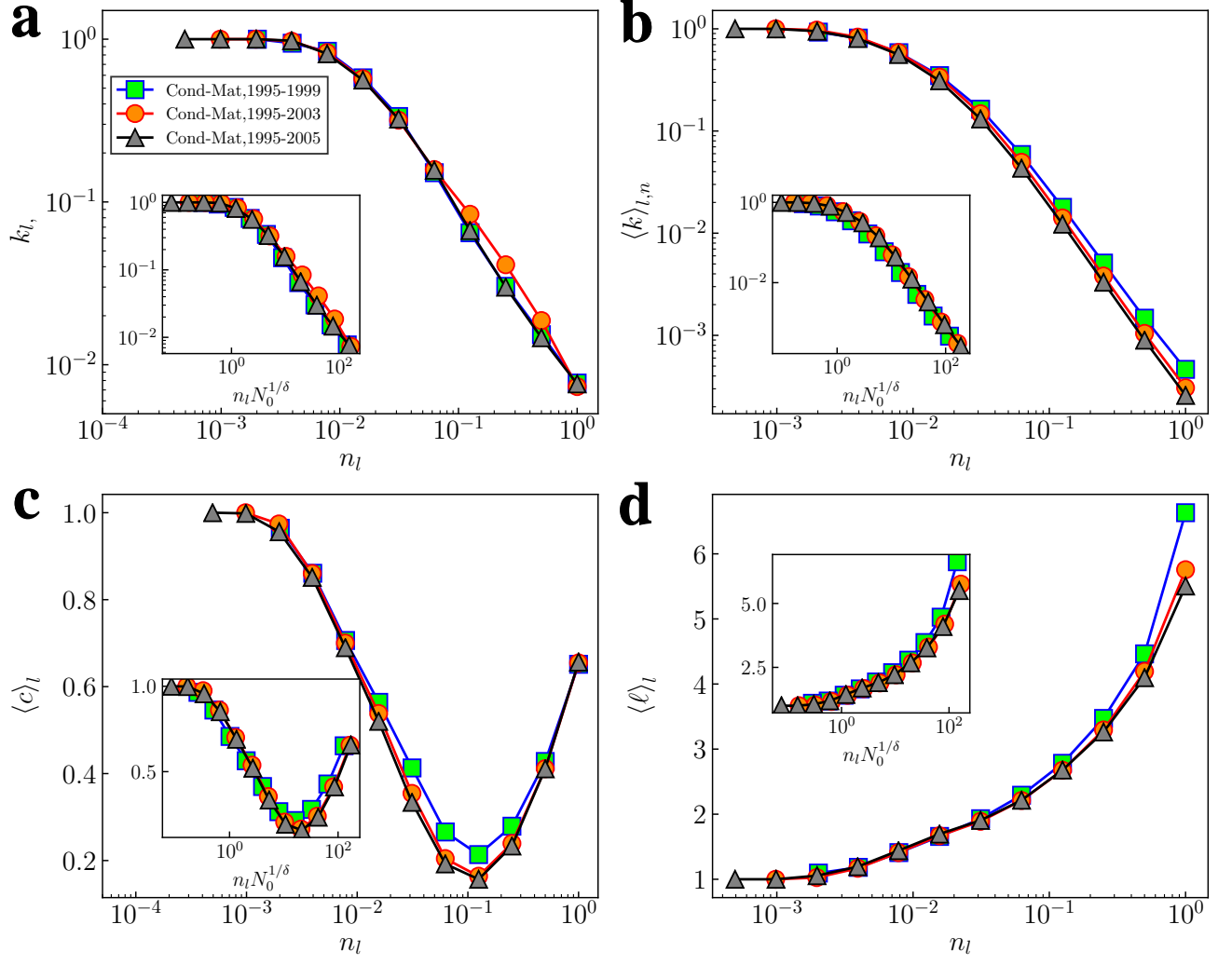


FIG. S34. FSS analysis of Condensed matter collaborations evolutionary networks' topological observables along the GR flow. The main figures show each observable as a function of the variable n_l in the process of GR transformation, and the inset shows their scaling functions related to the variable $n_l N_0^{1/\delta}$. These networks belong to phase **I**, and the scaling exponent corresponding to four observables is $\delta = 2 \pm 0.1$.

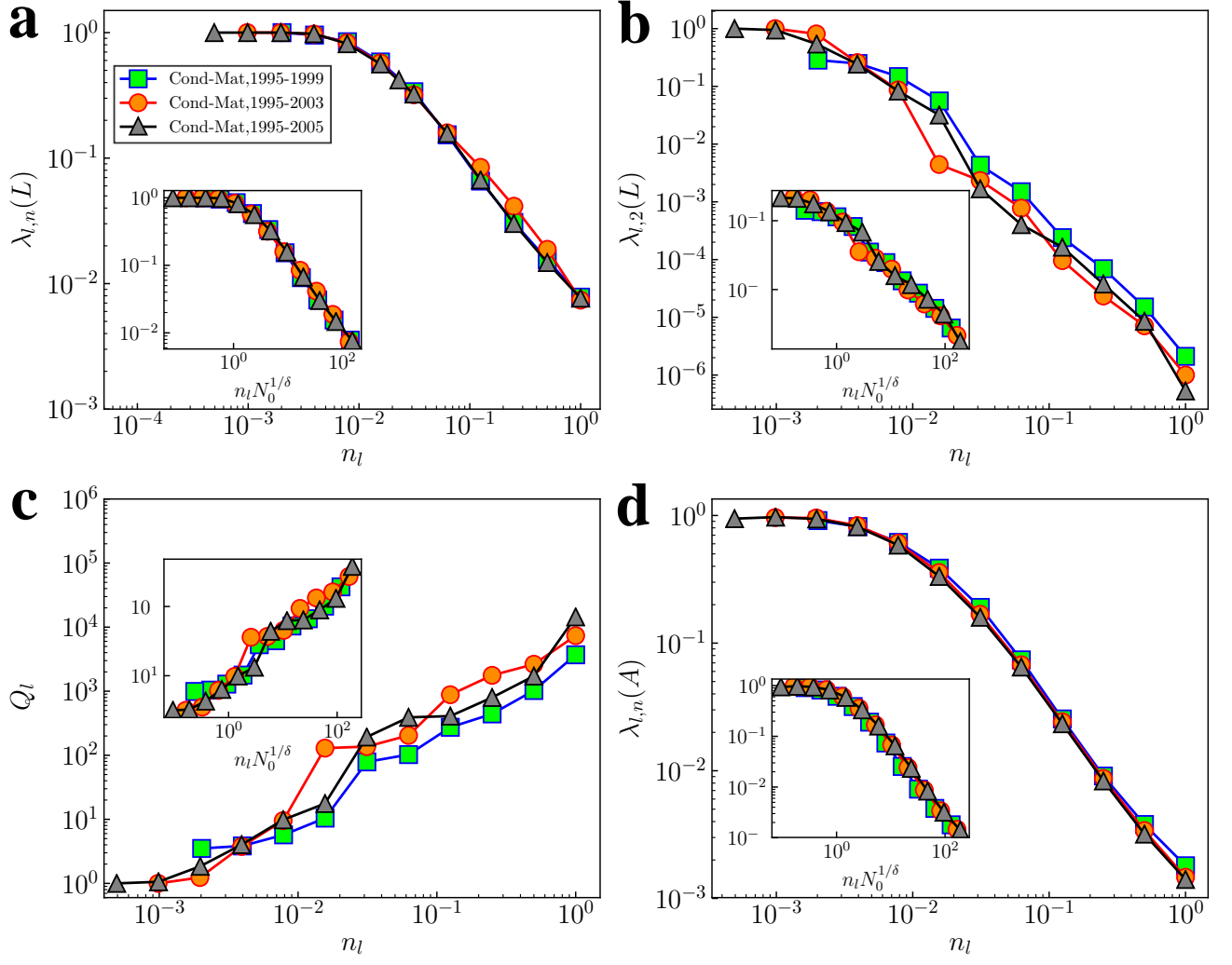


FIG. S35. FSS analysis of Condensed matter collaborations evolutionary networks' dynamical observables along the GR flow. The main figures show each observable as a function of the variable n_l in the process of GR transformation, and the inset shows their scaling functions related to the variable $n_l N_0^{1/\delta}$. The scaling exponent corresponding to four observables is $\delta = 2 \pm 0.1$.

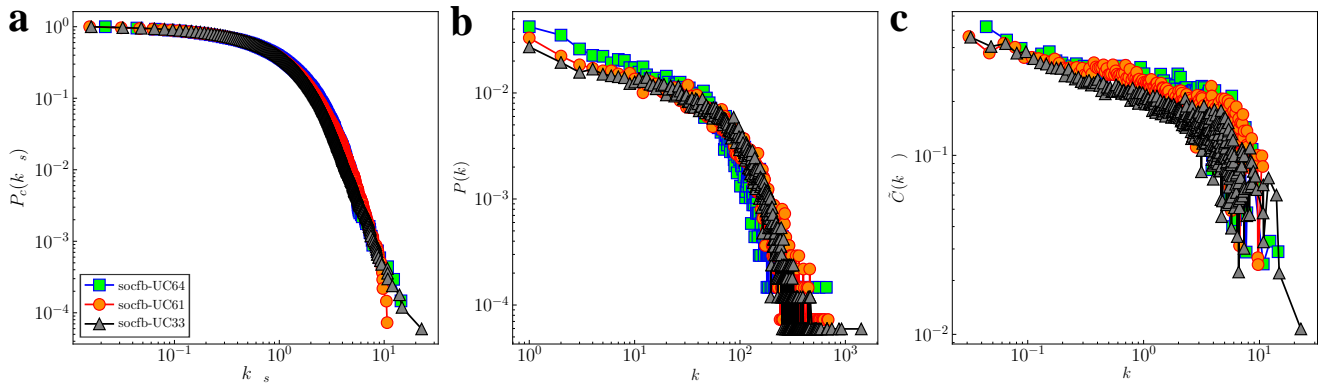


FIG. S36. Self-similarity of Socfb-UC evolutionary networks. a The complementary cumulative distribution function (CCDF) P_c of node rescaled degrees $k_{res} = k/\langle k \rangle$. b The probability distribution function (PDF) $P(k)$ of the degree of nodes. c The degree-dependent clustering coefficient $\tilde{C}(k_{res})$ of node rescaled degrees k_{res} . Topological characteristics of this series of evolutionary networks are given in Table S3.

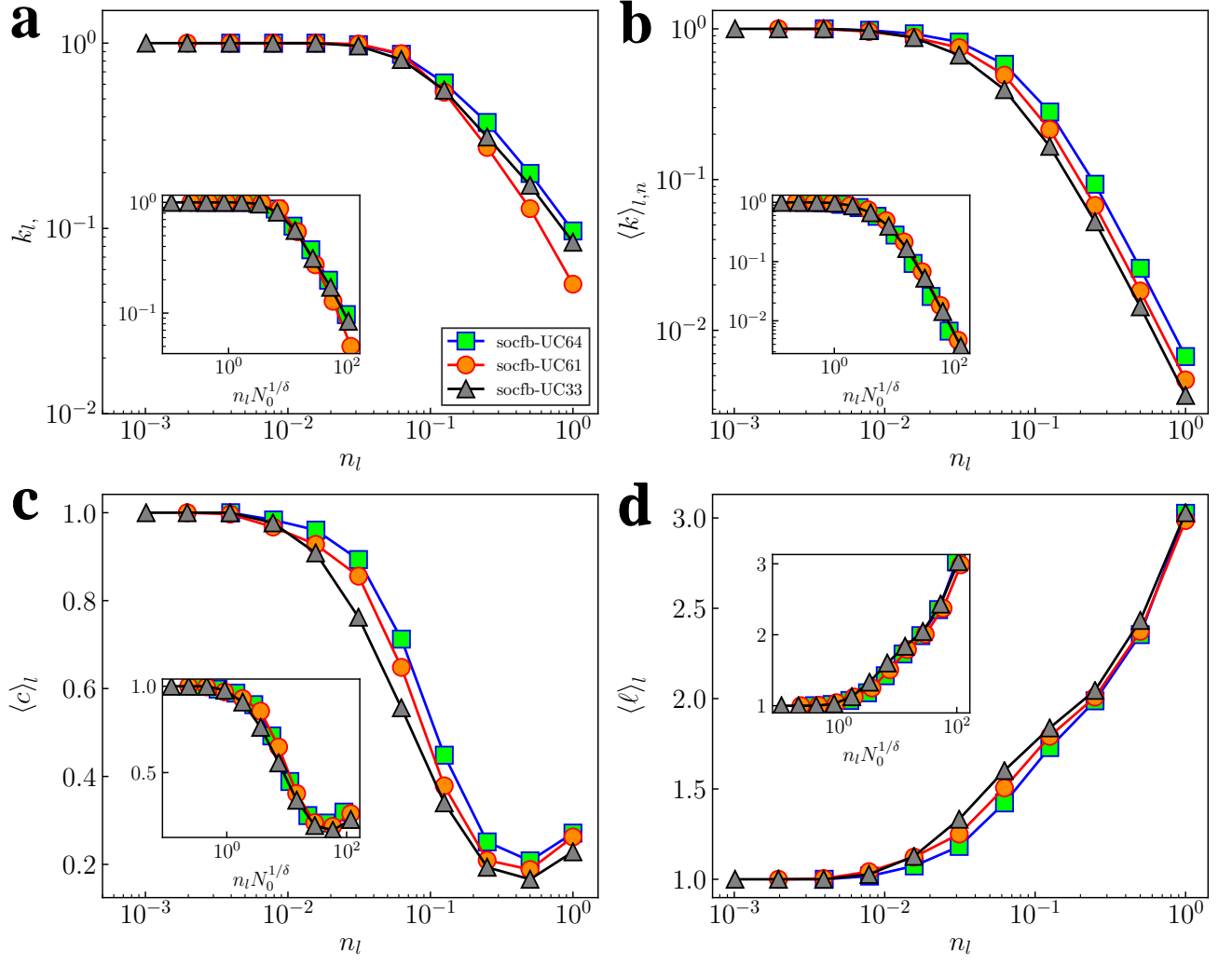


FIG. S37. FSS analysis of Socfb-UC evolutionary networks' topological observables along the GR flow. The main figures show each observable as a function of the variable n_l in the process of GR transformation, and the inset shows their scaling functions related to the variable $n_l N_0^{1/\delta}$. These networks belong to phase I, and the scaling exponent corresponding to four observables is $\delta = 2 \pm 0.1$.

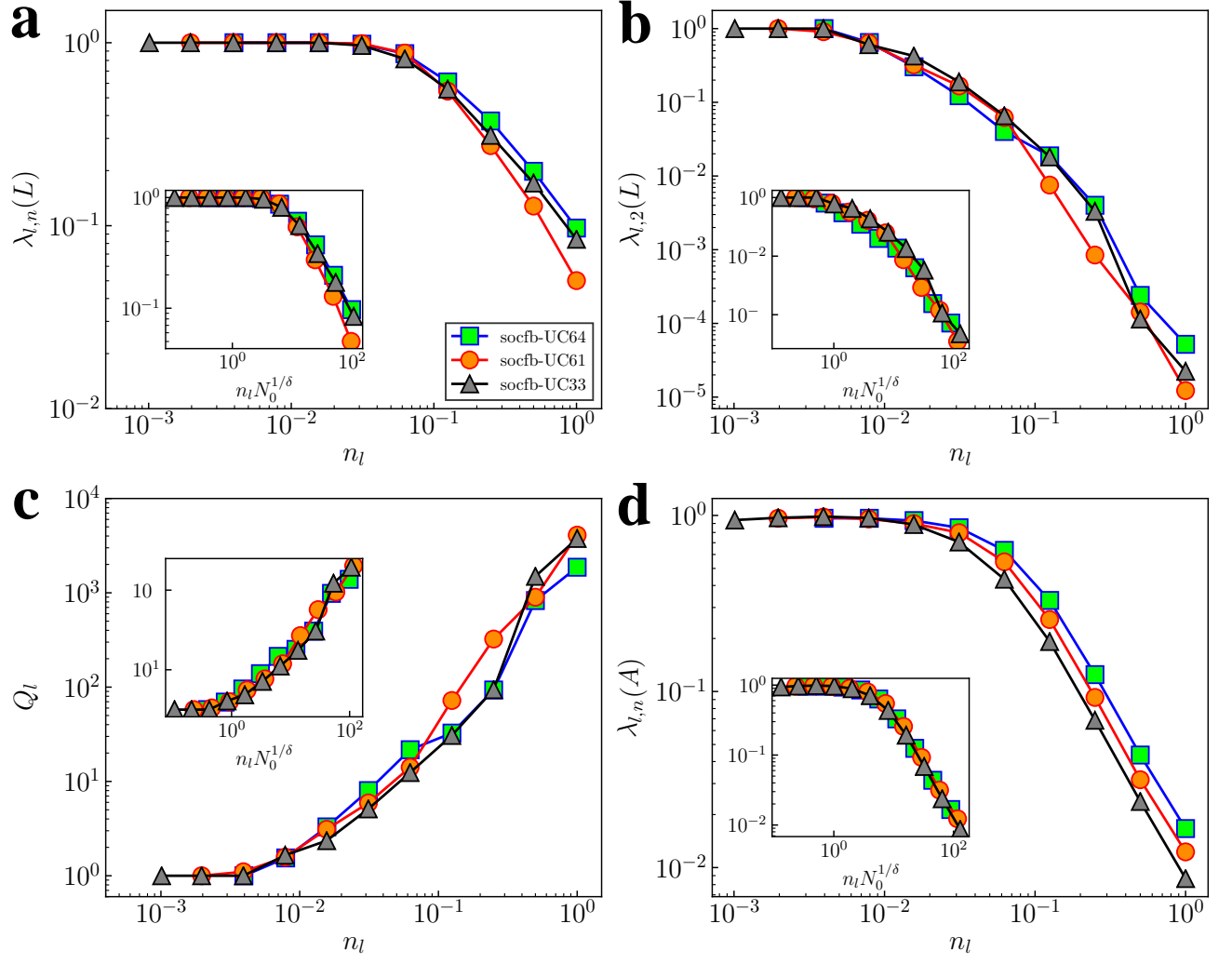


FIG. S38. FSS analysis of Socfb-UC evolutionary networks' dynamical observables along the GR flow. The main figures show each observable as a function of the variable n_l in the process of GR transformation, and the inset shows their scaling functions related to the variable $n_l N_0^{1/\delta}$. The scaling exponent corresponding to four observables is $\delta = 2 \pm 0.1$.

-
- [1] Serrano, M. Á., Krioukov, D. & Boguñá, M. Self-similarity of complex networks and hidden metric spaces. *Phys. Rev. Lett.* **100**, 078701 (2008).
 - [2] Krioukov, D., Papadopoulos, F., Vahdat, A. & Boguñá, M. Curvature and temperature of complex networks. *Phys. Rev. E* **80**, 035101(R) (2009).
 - [3] Krioukov, D., Papadopoulos, F., Kitsak, M., Vahdat, A. & Boguñá, M. Hyperbolic geometry of complex networks. *Phys. Rev. E* **82**, 036106 (2010).
 - [4] Papadopoulos, F., Kitsak, M., Serrano, M. Á., Boguñá, M. & Krioukov, D. Popularity versus similarity in growing networks. *Nature* **489**, 537-540 (2012).
 - [5] García-Pérez, G., Boguñá, M. & Serrano, M. Á. Multiscale unfolding of real networks by geometric renormalization. *Nat. Phys.* **14**, 583-589 (2018).
 - [6] Leskovec, J., Kleinberg, J. & Faloutsos, C. Graph evolution: densification and shrinking diameters. *ACM Trans. Knowl. Discov. Data (ACM TKDD)*, vol. 1, 2 (ACM, 2007).
 - [7] Ripeanu, M., Foster, I. & Iamnitchi, A. Mapping the gnutella network: properties of large-scale peer-to-peer systems and implications for system design. *IEEE Internet Comput.* (2002).
 - [8] Leskovec, J., Kleinberg, J. & Faloutsos, C. Graphs over time: densification laws, shrinking diameters and possible explanations. In *Proc. 17th ACM SIGKDD Int. Conf. on Knowl. Discov. Data Min.* 177-187 (ACM, 2005).
 - [9] Newman, M. E. The structure of scientific collaboration networks. *Proc. Natl. Acad. Sci. USA* **98**, 404-409 (2001).
 - [10] Rossi, R. A. & Ahmed, N. K. The network data repository with interactive graph analytics and visualization. *Proc. 29th AAAI Conf. on Artif. Intell.* (2015), <http://networkrepository.com>.
 - [11] García-Pérez, G., Allard, A., Serrano, M. Á. & Boguñá, M. Mercator: uncovering faithful hyperbolic embeddings of complex networks. *New J. Phys.* **21**, 123033 (2019).